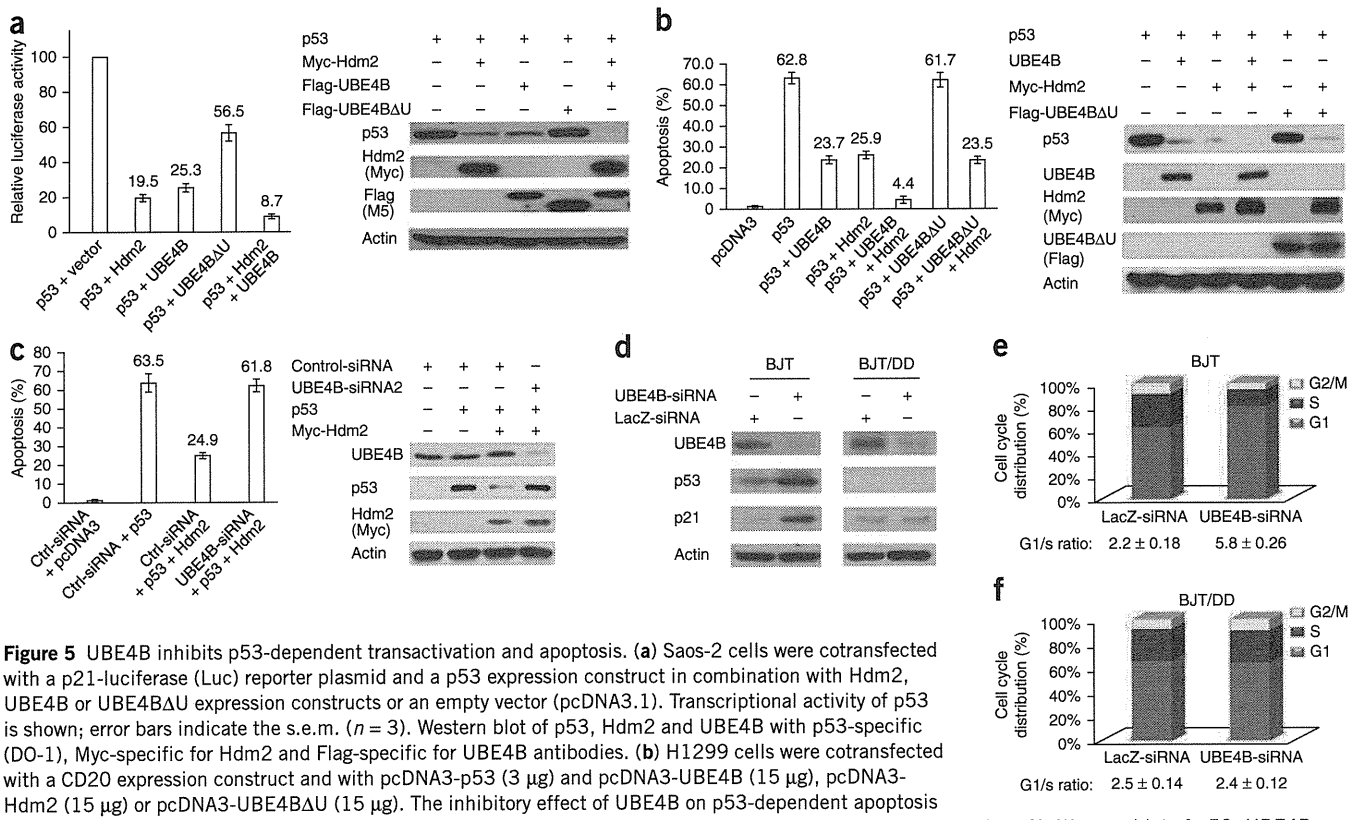

Figure 5 UBE4B inhibits p53-dependent transactivation and apoptosis. (**a**) Saos-2 cells were cotransfected with a p21-luciferase (Luc) reporter plasmid and a p53 expression construct in combination with Hdm2, UBE4B or UBE4BΔU expression constructs or an empty vector (pcDNA3.1). Transcriptional activity of p53 is shown; error bars indicate the s.e.m. ($n = 3$). Western blot of p53, Hdm2 and UBE4B with p53-specific (DO-1), Myc-specific for Hdm2 and Flag-specific for UBE4B antibodies. (**b**) H1299 cells were cotransfected with a CD20 expression construct and with pcDNA3-p53 (3 μg) and pcDNA3-UBE4B (15 μg), pcDNA3-Hdm2 (15 μg) or pcDNA3-UBE4BΔU (15 μg). The inhibitory effect of UBE4B on p53-dependent apoptosis was determined by annexin V staining of CD20-positive cells and flow cytometry. Error bars indicate the s.e.m. ($n = 3$). Western blot of p53, UBE4B, Hdm2 and UBE4BΔU with p53-specific (DO-1), UBE4B-specific, Myc-specific for Hdm2 and Flag-specific for UBE4BΔU antibodies. (**c**) H1299 cells were transfected with the UBE4B-siRNA or control-siRNA for 30 h. The cells were then transfected with the p53 expression construct alone or in combination with the Hdm2 and CD20 expression plasmids. The number of surviving CD20-positive cells was measured by flow cytometry 24 h after transfection. Error bars indicate the s.e.m. ($n = 3$). Western blot of UBE4B, p53 and Hdm2 with UBE4B-specific, p53-specific (DO-1) and Myc-specific antibodies. (**d**) Depletion of UBE4B by siRNA in BJT and BJT/DD cells, analyzed by western blotting with UBE4B-specific, p53-specific (DO-1) and p21-specific antibodies. (**e**,**f**). BJT (**e**) or BJT/DD (**f**) cells were treated with the LacZ-siRNA or UBE4B-siRNA2, and cell-cycle profile was determined by propidium iodide staining and flow cytometry. G1/s ratio is the ratio of subpopulations and G1-S phase fractions; it indicates the degree of G1 arrest. An antibody to β-actin (actin) was used as a loading control in panels **a**–**d**. Results represent the average of triplicate experiments.

a strong inverse correlation between elevated UBE4B expression and low or undetectable p53 expression ($P < 0.05$, Pearson correlation test). One human ependymoma tissue (NS61) and one pediatric astrocytoma tissue (NS006) had low UBE4B; the two tumor samples had elevated levels of p53 protein (**Fig. 6i,j**). According to mutational analysis, *UBE4B* is infrequently mutated in neuroblastoma and neuroblastoma-derived cell lines[26]. We identified mutations in *TP53* in human medulloblastoma DAOY (elevated p53) and UW228 cell lines, but no mutations of *TP53*, *MDM2* (encoding Hdm2; also known as *Hdm2*) or *UBE4B* in other tumor samples (data not shown). Although we observed upregulation of Hdm2 in some samples with low p53 expression, we detected no substantial *MDM2* gene amplification. These data suggest that Hdm2 is upregulated by mechanisms other than *MDM2* amplification and that p53 stabilization in p53 wild-type tumors may be mediated by the deregulation of UBE4B. Moreover, UBE4B overexpression was inversely correlated with low amount of p53 protein in most of the examined brain tumor samples we analyzed; however, the relationship is not completely reciprocal, because some tumors have decreased UBE4B (**Fig. 6**). Our findings indicate that additional factors may be involved in the formation of these tumors.

To investigate whether gene amplification is a mechanism of UBE4B protein overexpression in brain tumors, we evaluated the copy number of the *UBE4B* gene by real-time quantitative PCR. The *UBE4B* gene was amplified in 44–67% of various types of brain tumors (**Supplementary Fig. 7a–e**). This finding was further confirmed by Southern blot analysis (**Supplementary Fig. 7f–j**). We then used real-time PCR to show that *UBE4B* mRNA was overexpressed in most tumor samples (**Supplementary Fig. 8a–e**). We found a statistically significant relationship between *UBE4B* gene amplification and *UBE4B* mRNA overexpression ($P < 0.05$, Fisher's exact test (two-sided)). Thus, UBE4B overexpression is often associated with its gene amplification.

DISCUSSION

TP53 is rarely mutated in medulloblastoma and ependymoma[38,39]. Previous studies have reported that *MDM2* amplification is also uncommon in medulloblastoma and ependymoma[40]. Recent genetic mouse models showed that the loss of p53 accelerates medulloblastoma development[41,42], indicating that the p53 pathway is indeed inactivated in these tumors. However, the mechanism underlying the inactivation of the p53 pathway in brain tumors remains unclear. Mdm2 mediates only the mono- or multiple-monoubiquitination of p53, and it has been proposed that cofactors are required for Mdm2 to promote p53 polyubiquitination and degradation[15–18]. In this study, we report that UBE4B is essential and required for Hdm2-mediated p53 polyubiquitination and degradation.

Mdm2 promotes p53 degradation[7–9], but the mechanisms by which it does so are poorly understood. Here we showed that UBE4B overexpression greatly decreased the amount of p53 protein in various

types of cells and that ablation of UBE4B stabilized the p53 protein. Either Mdm2 or Ube4b alone mediated the monoubiquitination of p53 *in vitro*, while Ube4b, in combination with Mdm2, promoted p53 polyubiquitination *in vitro*. Furthermore, UBE4B can repress p53-dependent transactivation and apoptosis. Elevated UBE4B protein expression has been observed in several brain tumors and various medulloblastoma cell lines (**Fig. 6**). Most notably, we observed an inverse correlation between UBE4B overexpression and low p53 expression in these brain tumors. Our data indicate that amplification and overexpression of *UBE4B* represent a previously undescribed molecular mechanism of inactivation of p53 in brain tumors and that inhibition of UBE4B activity could represent a new approach to the treatment of brain cancer.

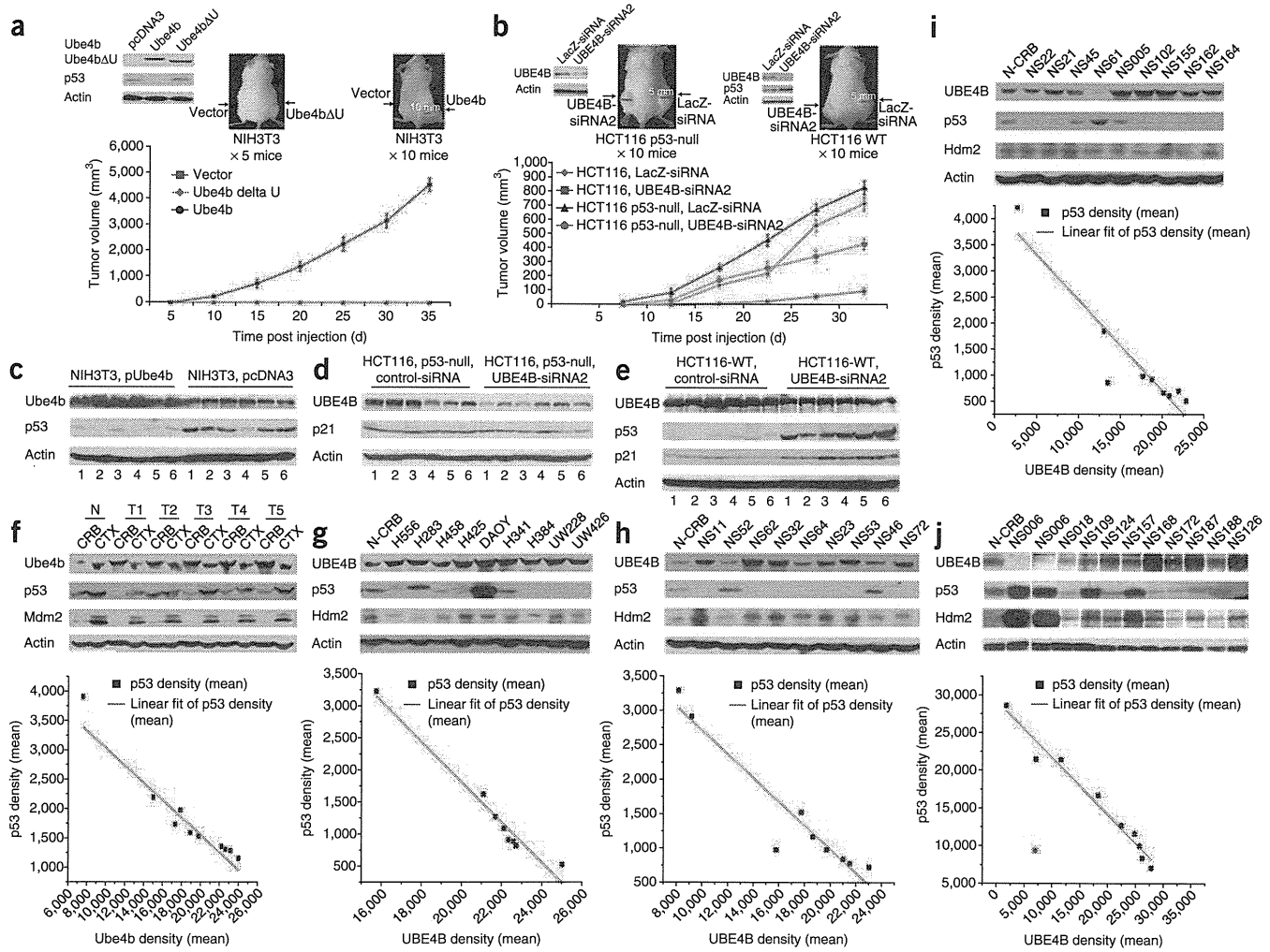

Figure 6 UBE4B promotes tumorigenesis in a p53-dependent manner and is overexpressed in brain tumors. (**a**) 1×10^7 NIH3T3 cells expressing Flag-Ube4b or Flag-Ube4bΔU or an empty vector were subcutaneously injected into SCID mice. A portion of the transfected NIH3T3 cells was lysed and analyzed by western blotting as indicated. The tumor volume (mm^3) was estimated from caliper measurements. The difference of the population means of the Ube4b-injected group is significantly different compared to the empty vector– and Ube4bΔU-injected groups ($P < 0.01$, one-way ANOVA). Error bars show s.d. ± the mean volume of ten xenografts. (**b**) 1×10^7 HCT116 *TP53*$^{-/-}$ cells expressing the control siRNA or UBE4B-siRNA2 were subcutaneously injected into SCID mice as indicated (left). A portion of the transfected HCT116 *TP53*$^{-/-}$ cells was lysed and analyzed by western blotting as indicated. Similarly, HCT116-WT cells were used as the tumor cells (right). Tumor size volumes from four different injected groups were analyzed by two-way ANOVA ($P < 0.01$). Error bars show the s.d. from the mean volume of ten xenografts. (**c**–**e**) Six tumor samples from each group mice were dissected 35 d (**c**) or 30 d (**d**,**e**) after injection and analyzed by western blotting with the indicated antibodies. (**f**) Representative western blot analysis of mouse medulloblastoma tissues derived from *Ptch*$^{+/-}$ mice. Proteins were extracted from mouse cerebellum (CRB) and cortex (CTX) and then analyzed by western blotting with indicated antibodies. N denotes normal mouse tissue, and T denotes tumor tissue. The inverse correlation between the amounts of p53 protein that of Ube4b protein was tested with a Pearson correlation test. $y = -0.14881x + 4525.41$; Pearson correlation: −0.96716; significance (two-tailed test): 4.89362×10^{-6}. (**g**) Whole-cell extracts of medulloblastoma cell lines were analyzed by western blotting with the indicated antibodies. The inverse correlation between the amounts of p53 protein and the amounts of UBE4B protein was tested with a Pearson correlation test. $y = -0.31433x + 8103.88862$; Pearson correlation: −0.98241; significance (two-tailed test): 1.3423×10^{-5}. (**h**) Similar to **f** and **g** except that proteins were prepared from human medulloblastoma tissues. NS is the prefix for the USA national tissue bank number. The inverse correlation between p53 and UBE4B protein levels was tested with a Pearson correlation test. $y = -0.17304x + 4440.7514$; Pearson correlation: −0.95033; significance (two-tailed test): 8.56558×10^{-5}. (**i**) Similar to **h** except that proteins were prepared from human ependymoma. The inverse correlation between amount of p53 and UBE4B protein was tested with a Pearson correlation test. $y = -0.17442x + 4192.60377$; Pearson correlation: −0.93287; significance (two-tailed test): 2.41633×10^{-4}. (**j**) Similar to **h** and **i** except that proteins were prepared from pediatric astrocytoma. The inverse correlation between p53 protein level and UBE4B protein level was tested with a Pearson correlation test. $y = -0.75587x + 29275.47726$; Pearson correlation: −0.98423; significance (two-tailed test): 1.59542×10^{-6}. An antibody to β-actin (actin) was used as a loading control in panels **c**–**j**.

Recently, YY1, CREB-binding protein (CBP) and E1A binding protein p300 (p300) were reported as E4 ligases that mediate p53 polyubiquitination in humans[17,31,32]. Although CBP is required for p53 polyubiquitination *in vivo*, it shows an Mdm2-independent, p53-directed E4 ligase function[31]. YY1 was described as a molecular clamp to mediate p53 polyubiquitination[32]. In contrast, UBE4B is a U-box–containing E3/E4 ubiquitin ligase. Unlike CBP, UBE4B depends mainly on Hdm2 for its E4 ligase activity for p53. CBP and p300 are E4 ligases and act only on previously monoubiquitinated substrates[31]; however, UBE4B requires functional Hdm2 to promote degradation of p53. Thus, it is possible that p53 is targeted for polyubiquitination by different pathways and regulated through different mechanisms.

Overall, we have identified UBE4B as an E4 ligase that is essential for Hdm2 to promote p53 polyubiquitination and degradation. Furthermore, our findings show that UBE4B is overexpressed in various brain tumors, and they reveal a new link between the tumor suppressor p53 and the oncogene *MDM2*. Thus, these findings have considerable implications for cancer therapy.

METHODS

Methods and any associated references are available in the online version of the paper at http://www.nature.com/naturemedicine/.

Note: Supplementary information is available on the Nature Medicine website.

ACKNOWLEDGMENTS

We gratefully acknowledge W. Gu (Columbia University) for the His-ubiquitin (wild-type) and His-Ub-ko plasmids, A.G. Jochemsen (Erasmus University Medical Center) for the Myc-Mdm2 plasmid, C. Blattner (Universität Heidelberg) for pSuper.neo.gpf-Mdm2 siRNA plasmid, J.A. Mahoney (Johns Hopkins University) for pEF-DEST51-Flag-UBE4B plasmid, B. Vogelstein (Johns Hopkins University) for HCT116 *TP53*$^{-/-}$ cells, S. Benchimol (York University) for BJT and BJT/DD cell lines and G. Lozano (University of Texas, M.D. Anderson Cancer Center) for *Mdm2*$^{-/-}$ *Trp53*$^{-/-}$ MEFs as described in the text. We thank T. Turner for technical help in making the figures. This work was supported by grants from the Alberta Heritage Foundation for Medical Research and Canadian Institutes of Health Research (to R.P.L.) and from the US National Institutes of Health (to S.L.P.). R.P.L. is an Alberta Heritage Foundation for Medical Research scholar.

AUTHOR CONTRIBUTIONS

H.W. and R.P.L. contributed to study design, performed most of the experiments, analyzed and interpreted the data and wrote the manuscript. S.L.P. provided logistical support and all tumor samples and interpreted and discussed the data. M.F. provided technical support and experimental assistance. N.T. conducted the western blotting for the pediatric astrocytoma tissues, isolated genomic DNAs from various tumor samples, carried out mutation detection for p53 in various tumor tissues and medulloblastoma cell lines and did long-term colony assays. J.M. collected tissue samples from various types of human brain tumors, cared for *Ptch*$^{+/-}$ mice, conducted all the mouse genotyping and isolated the cerebellum and cortex from the *Ptch*$^{+/-}$ mice. K.I.N. and S.H. provided the study material and technical support. V.A.T. provided technical support. L.F.S. conducted the FPLC protein purification experiments. L.S. provided technical support for the gel filtration. R.P.L. supervised and directed the project.

COMPETING FINANCIAL INTERESTS

The authors declare no competing financial interests.

Published online at http://www.nature.com/naturemedicine/.
Reprints and permissions information is available online at http://npg.nature.com/reprintsandpermissions/.

1. Farrell, P.J., Allan, G.J., Shanahan, F., Vousden, K.H. & Crook, T. p53 is frequently mutated in Burkitt's lymphoma cell lines. *EMBO J.* **10**, 2879–2887 (1991).
2. Crook, T. & Vousden, K.H. Properties of p53 mutations detected in primary and secondary cervical cancers suggest mechanisms of metastasis and involvement of environmental carcinogens. *EMBO J.* **11**, 3935–3940 (1992).
3. Greenblatt, M.S., Bennet, W.P., Hollstein, M. & Harris, C.C. Mutations in the p53 tumor suppressor gene: Clues to cancer etiology and molecular pathogenesis. *Cancer Res.* **54**, 4855–4878 (1994).
4. Levine, A.J. p53, the cellular gatekeeper for growth and division. *Cell* **88**, 323–331 (1997).
5. Vogelstein, B., Lane, D. & Levine, A.J. Surfing the p53 network. *Nature* **408**, 307–310 (2000).
6. Donehower, L.A. *et al.* Mice deficient for p53 are developmentally normal but susceptible to spontaneous tumours. *Nature* **356**, 215–221 (1992).
7. Haupt, Y., Maya, R., Kazaz, A. & Oren, M. Mdm2 promotes the rapid degradation of p53. *Nature* **387**, 296–299 (1997).
8. Kubbutat, M.H., Jones, S.N. & Vousden, K.H. Regulation of p53 stability by Mdm2. *Nature* **387**, 299–303 (1997).
9. Honda, R., Tanaka, H. & Yasuda, Y. Oncoprotein MDM2 is a ubiquitin ligase E3 for tumor suppressor p53. *FEBS Lett.* **420**, 25–27 (1997).
10. Montes de Oca Luna, R., Wagner, D.S. & Lozano, G. Rescue of early embryonic lethality in mdm2-deficient mice by deletion of p53. *Nature* **378**, 203–206 (1995).
11. Jones, S.N., Roe, A.E., Donehower, L.A. & Bradley, A. Rescue of embryonic lethality in Mdm2-deficient mice by absence of p53. *Nature* **378**, 206–208 (1995).
12. Piotrowski, J. *et al.* Inhibition of the 26 S proteasome by polyubiquitin chains synthesized to have defined lengths. *J. Biol. Chem.* **272**, 23712–23721 (1997).
13. Thrower, J.S., Hoffman, L., Rechsteiner, M. & Pickart, C.M. Recognition of the polyubiquitin proteolytic signal. *EMBO J.* **19**, 94–102 (2000).
14. Pickart, C.M. Ubiquitin in chains. *Trends Biochem. Sci.* **25**, 544–548 (2000).
15. Rodriguez, M.S., Desterro, J.M., Lain, S., Lane, D.P. & Hay, R.T. Multiple C-terminal lysine residues target p53 for ubiquitin-proteasome-mediated degradation. *Mol. Cell. Biol.* **20**, 8458–8467 (2000).
16. Lai, Z. *et al.* Human mdm2 mediates multiple mono-ubiquitination of p53 by a mechanism requiring enzyme isomerization. *J. Biol. Chem.* **276**, 31357–31367 (2001).
17. Grossman, S.R. *et al.* Polyubiquitination of p53 by a ubiquitin ligase activity of p300. *Science* **300**, 342–344 (2003).
18. Li, M. *et al.* Mono- versus polyubiquitination: differential control of p53 fate by Mdm2. *Science* **302**, 1972–1975 (2003).
19. Johnson, E.S., Ma, P.C.M., Ota, I. & Varshavsky, A. A proteolytic pathway that recognizes ubiquitin as a degradation signal. *J. Biol. Chem.* **270**, 17442–17456 (1995).
20. Koegl, M. *et al.* A novel ubiquitination factor, E4, is involved in multiubiquitin chain assembly. *Cell* **96**, 635–644 (1999).
21. Hatakeyama, S., Yada, M., Matsumoto, M., Ishida, N. & Nakayama, K.I. U box proteins as a new family of ubiquitin-protein ligases. *J. Biol. Chem.* **276**, 33111–33120 (2001).
22. Tu, D., Li, W., Ye, Y. & Brunger, A.T. Structure and function of the yeast U-box-containing ubiquitin ligase Ufd2p. *Proc. Natl. Acad. Sci. USA* **104**, 15599–15606 (2007).
23. Koepp, D.M., Harper, J.W. & Elledge, S.J. How the cyclin became a cyclin: regulated proteolysis in the cell cycle. *Cell* **97**, 431–434 (1999).
24. Matsumoto, M. *et al.* Molecular clearance of ataxin-3 is regulated by a mammalian E4. *EMBO J.* **23**, 659–669 (2004).
25. Okumura, F., Hatakeyama, S., Matsumoto, M., Kamura, T. & Nakayama, K.I. Functional regulation of FEZ1 by the U-box–type ubiquitin ligase E4B contributes to neuritogenesis. *J. Biol. Chem.* **279**, 53533–53543 (2004).
26. Hosoda, M. *et al.* UFD2a mediates the proteasomal turnover of p73 without promoting p73 ubiquitination. *Oncogene* **24**, 7156–7169 (2005).
27. Kaneko-Oshikawa, C. *et al.* Mammalian E4 is required for cardiac development and maintenance of the nervous system. *Mol. Cell. Biol.* **25**, 10953–10964 (2005).
28. Leng, R.P. *et al.* Pirh2, a p53 induced ubiquitin-protein ligase, promotes p53 degradation. *Cell* **112**, 779–791 (2003).
29. Sheng, Y. *et al.* Molecular basis of Pirh2-mediated p53 ubiquitylation. *Nat. Struct. Mol. Biol.* **15**, 1334–1342 (2008).
30. Dornan, D. *et al.* The ubiquitin ligase COP1 is a critical negative regulator of p53. *Nature* **429**, 86–92 (2004).
31. Shi, D. *et al.* CBP and p300 are cytoplasmic E4 polyubiquitin ligases for p53. *Proc. Natl. Acad. Sci. USA* **106**, 16275–16280 (2009).
32. Sui, G. *et al.* Yin Yang 1 is a negative regulator of p53. *Cell* **117**, 859–872 (2004).
33. Finlay, C.A. The mdm-2 oncogene can overcome wild-type p53 suppression of transformed cell growth. *Mol. Cell. Biol.* **13**, 301–306 (1993).
34. McCurrach, M.E., Connor, T.M., Knudson, C.M., Korsmeyer, S.J. & Lowe, S.W. bax-deficiency promotes drug resistance and oncogenic transformation by attenuating p53-dependent apoptosis. *Proc. Natl. Acad. Sci. USA* **94**, 2345–2349 (1997).
35. Serrano, M., Lin, A.W., McCurrach, M.E., Beach, D. & Lowe, S.W. Oncogenic *ras* provokes premature cell senescence associated with accumulation of p53 and p16INK4a. *Cell* **88**, 593–602 (1997).
36. Waldman, T. *et al.* Cell-cycle arrest versus cell death in cancer therapy. *Nat. Med.* **3**, 1034–1036 (1997).
37. Bunz, F. *et al.* Requirement for p53 and p21 to sustain G_2 arrest after DNA damage. *Science* **282**, 1497–1501 (1998).
38. Saylors, R.L. *et al.* Infrequent p53 gene mutations in medulloblastomas. *Cancer Res.* **51**, 4721–4723 (1991).
39. Gaspar, N. *et al.* p53 Pathway dysfunction in primary childhood ependymomas. *Pediatr. Blood Cancer* **46**, 604–613 (2006).
40. Adesina, A.M., Nalbantoglu, J. & Cavenee, W.K. p53 gene mutation and mdm2 gene amplification are uncommon in medulloblastoma. *Cancer Res.* **54**, 5649–5651 (1994).
41. Crawford, J.R., MacDonald, T.J. & Packer, R.J. Medulloblastoma in childhood: new biological advances. *Lancet Neurol.* **6**, 1073–1085 (2007).
42. Uziel, T. *et al.* The tumor suppressors Ink4c and p53 collaborate independently with Patched to suppress medulloblastoma formation. *Genes Dev.* **19**, 2656–2667 (2005).

ONLINE METHODS

Subject data. All tumor samples were collected at the time of initial diagnosis and before treatment with chemotherapy or radiation in the years 1995–2007 at Children's Hospital Boston. The samples were obtained after informed consent allowing use for the experiments in this study, as approved by the Institutional Review Board of Children's Hospital Boston and Harvard Medical School and the Research Ethics Board of the University of Alberta.

Plasmids and antibodies. Ube4b (also called Ufd2a in mouse and UBE4B in humans) or UBE4B or Ube4b mutants were cloned into pcDNA3.1 or p3x Flag-CMV-10 (Sigma-Aldrich), pET28a (Novagen), p21-Luc reporter plasmid described previously[28] or pBacPAK9 (Clontech)[21]. All PCR products were confirmed by sequencing. We used p53-specific antibodies (Pab421, Calbiochem; FL-393, Santa Cruz; DO-1, Abcam; CM5, Novocastra; Ab-7, Oncogene Research Products), Mdm2-specific antibodies (2A10, Calbiochem; SMP14, BD Biosciences; MD-219, Sigma-Aldrich), p21-specific antibody (F-5, Santa Cruz), Myc-tagged–specific antibody (9E10, Roche), Flag-tagged–specific antibodies (M5, M2, Sigma), HA-tagged–specific antibody (12CA5, Roche), ubiquitin-specific, CD20-specific and UFD2/E4-specific antibodies (BD Biosciences), actin-specific antibody (Sigma-Aldrich), PRP19-specific, UBE1-specific and UbcH5b-specific antibodies (Abcam), and polyclonal antibodies for Ube4b (ref. 21).

Yeast two-hybrid screen. Yeast strain AH109 was transformed with the plasmid pAS2-1-Mdm2 and a mouse brain cDNA library in the pACT2 vector (Clontech). Approximately 6×10^7 transformants were screened, and 20 positive clones were isolated after two rounds of growth in the absence of histidine, adenine and screening for β-galactosidase activity. Recovered plasmids from AH109 were used to cotransform Y190 yeast with either full-length Mdm2 or Mdm2 mutants.

Gel filtration. Cell lysates were fractioned with a fast protein liquid chromatography protein purification system on a Superose 6 column (GE Healthcare). The column was equilibrated with Tris buffer (50 mM Tris, pH7.5, 150 mM NaCl, 0.1% (vol/vol) Triton X-100), and lysates (2 mg) were applied to and eluted from the column with the same buffer. The flow rate was 0.4 ml min^{-1}, and 380 μl fractions were collected. The column was calibrated with Bio-Rad gel filtration standards containing thyroglobulin (670 kDa), γ-globulin (158 kDa), ovalbumin (44 kDa), myoglobin (17 kDa) and Vitamin B_{12} (1.3 kDa).

siRNA experiments. We examined six pairs of Ube4b-siRNA. We found that siRNA-2562 (named Ube4b-siRNA1, 5′-CAGCGAGTTCTATGAC AAG-3′) and siRNA-3263 (named Ube4b-siRNA2, 5′-AGAATGCGCGGGCAG AAAT-3′) effectively knocked down endogenous Ube4b. Similarly, we tested six pairs of UBE4B-siRNA and found that the UBE4B-siRNA1 (5′-GCA ACTAGACACCGCGAAA-3′) and UBE4B-siRNA2 (5′-CCCTGTGTGCA ATTTGGTT-3′) effectively knocked down endogenous UBE4B in various human cell lines. pSuper.neo.gfp-Mdm2 siRNA (5′-GACAAAGAAGAGA GTGTGG-3′) was a kind gift from C. Blattner.

Generation of knockdown cell lines. The 19-nucleotide oligonucleotides derived from UBE4B-siRNA1, UBE4B-siRNA2, Ube4b-siRNA1 and Ube4b-siRNA2 were cloned into pSuper.puro vector according to the manufacturer's instructions (OligoEngine). To obtain insight into the function of UBE4B or Ube4b, several cell lines were transfected with the plasmids expressing UBE4B-siRNA or Ube4b-siRNA and selected in hygromycine for 2 weeks; thereafter, independent stable clones were selected and evaluated by western blotting.

***In vitro* ubiquitination assay.** The *in vitro* ubiquitination assay was performed as described previously[28]. For the coupled *in vitro* ubiquitination-immunoprecipitation assay, purified His-p53 protein (200 ng) was preincubated with His-Mdm2 protein (200 ng) on ice for 30 min before incubation with ubiquitin reaction components (E1, E2 and ubiquitin). The mixtures were incubated at 30 °C for 30 min to generate ubiquitinated p53. Purified His-Ube4b (300 ng) was then added and followed by additional incubation times, and then the mixtures were immunoprecipitated and analyzed. A One-step E4 assay was done, as described previously[17,31]. Baculovirus-expressed p53 and Flag-Mdm2 were purified as a complex with Flag M2 agarose (Sigma-Aldrich) and then incubated with ubiquitin reaction components at 30 °C for 30 min. Flag-Ube4b was immunopurified from baculovirus-infected sf9 insect cells (Clontech). The Sf9 cell line was derived from pupal ovarian tissue of the fall armyworm *Spodoptera frugiperda*. The Sf9 cell line is highly susceptible to infection with *Autographa california* nuclear polyhedrosis virus (AcNPV baculovirus), and can be used with all baculovirus expression vectors.) was added, followed by further incubation of the reaction at 30 °C for 60 min and analysis by immunoblotting.

***In vivo* ubiquitination assay.** This assay was performed as described previously[28].

Two-step E4 assay. This assay was performed as described previously[31]. Briefly, baculovirus-expressed HA-p53 was ubiquitinated by Flag-Hdm2. p53 was immunoprecipitated with beads conjugated with antibody to HA under stringent (RIPA buffer: 50 mM Tris-HCl, pH 7.4; 150 mM NaCl; 0.1% (wt/vol) SDS; 0.5% (wt/vol) Na-deoxycholate; 1% (wt/vol) Nonidet P40) conditions to remove Hdm2 and nontagged ubiquitin. The mixtures were washed three times with RIPA buffer, twice with PBS (137 mM NaCl; 2.7 mM KCl; 10 mM Na_2HPO_4; 2 mM KH_2PO_4; pH is adjusted to 7.4 with HCl), and twice with Ub buffer (50 mM Tris-HCl, pH 7.4; 2 mM ATP; 5 mM $MgCl_2$; 2 mM DTT). Immunobilized p53 was then mixed with second ubiquitination reaction components (50 ng E1, 100 ng UbcH5b, 5 μg Flag-tagged Ub) along with affinity-purified Flag-UBE4B or Flag-CBP obtained from transfected U2OS (human osteosarcoma; ATCC, HTB-96) cells and incubated at 30 °C for 60 min. To remove UBE4B autoubiquitination products, beads were washed three times with RIPA buffer and then analyzed by western blot with Flag-specific antibodies (M2 or M5, Sigma-Aldrich).

Xenograft growth assay. For tumorigenicity assay, 1×10^7 NIH3T3 cells (ATCC, CRL-1658) expressing Ube4b or Ube4bΔU or empty vector suspended in 0.2 ml HBSS (Invitrogen) were subcutaneously injected into the upper thigh of one or both legs of 6-week-old female SCID mice (Charles River). To examine whether elimination of UBE4B expression by siRNA could inhibit tumor growth, wild-type HCT116 or HCT116 *TP53*$^{-/-}$ cells were transfected with the pSUPER-UBE4B-siRNA2.puro or pSUPER-LacZ-siRNA.puro and selected with 2 μg ml^{-1} puromycin. Independent clones were selected and evaluated by western blotting. The selected clones were allowed to recover in the absence of puromycin. Subsequently, HCT116 or HCT116 *TP53*$^{-/-}$ tumor cells bearing UBE4B-siRNA or LacZ-siRNA were injected into the upper thigh of both legs of 6-week-old female SCID mice. The mice were monitored regularly for tumor growth. Tumor size was measured with a caliper.

Statistical analyses. Comparison the half-life of endogenous p53 between overexpressed Ube4b and overexpressed an empty vector or Ube4bΔU was performed with one-way analysis of variance (ANOVA) in OriginLab's Origin Pro 8 software (**Supplementary Fig. 4a–b**). Comparison the half-life of endogenous p53 between siControl and siMdm2 or siUbe4b or siMdm2 and siUbe4b was performed with two-way ANOVA in Origin Pro 8 software (**Supplementary Fig. 4d**). One-way ANOVA in Origin Pro 8 was also used to assess the relationship between Ube4b injected group and the empty vector or Ube4bΔU injected group (**Fig. 6a**). Two-way ANOVA in Origin Pro 8 was also used to assess the tumor size volumes from four different injected groups (**Fig. 6b**). The inverse/negative correlation between UBE4B and p53 protein levels was evaluated statistically by Pearson Correlation Test in Origin Pro 8. In addition, we conducted two-tailed test of significance with the same software (**Fig. 6f–j**). *UBE4B* gene amplification and *UBE4B* mRNA overexpression were calculated by Fisher's exact test (two-sided) in SPSS (PASW) software (**Supplementary Figs. 7a–e** and **8a–e**). The criterion we used to determine statistical significance was $P < 0.05$.

Additional methods. Detailed methodology is described in the **Supplementary Methods**.

doi:10.1038/nm.2283

OPEN ACCESS Freely available online

PLoS one

Nuclear Pore Complex Protein Mediated Nuclear Localization of Dicer Protein in Human Cells

Yoshinari Ando[1☯], Yasuhiro Tomaru[1☯], Ayako Morinaga[1], Alexander Maxwell Burroughs[1], Hideya Kawaji[1], Atsutaka Kubosaki[1], Ryuichiro Kimura[2], Maiko Tagata[2], Yoko Ino[3], Hisashi Hirano[3], Joe Chiba[2], Harukazu Suzuki[1], Piero Carninci[1], Yoshihide Hayashizaki[1]*

1 RIKEN Omics Science Center, Yokohama, Kanagawa, Japan, **2** Department of Biological Science and Technology, Tokyo University of Science, Noda, Chiba, Japan, **3** Supramolecular Biology, International Graduate School of Arts and Sciences, Yokohama City University, Yokohama, Kanagawa, Japan

Abstract

Human DICER1 protein cleaves double-stranded RNA into small sizes, a crucial step in production of single-stranded RNAs which are mediating factors of cytoplasmic RNA interference. Here, we clearly demonstrate that human DICER1 protein localizes not only to the cytoplasm but also to the nucleoplasm. We also find that human DICER1 protein associates with the NUP153 protein, one component of the nuclear pore complex. This association is detected predominantly in the cytoplasm but is also clearly distinguishable at the nuclear periphery. Additional characterization of the NUP153-DICER1 association suggests NUP153 plays a crucial role in the nuclear localization of the DICER1 protein.

Citation: Ando Y, Tomaru Y, Morinaga A, Burroughs AM, Kawaji H, et al. (2011) Nuclear Pore Complex Protein Mediated Nuclear Localization of Dicer Protein in Human Cells. PLoS ONE 6(8): e23385. doi:10.1371/journal.pone.0023385

Editor: Fatah Kashanchi, George Mason University, United States of America

Received April 4, 2011; **Accepted** July 15, 2011; **Published** August 15, 2011

Funding: This work was supported by Research Grant for RIKEN Omics Science Center from Ministry of Education, Culture, Sports, Science and Technology (MEXT) Japan to YH, Grant of the Innovative Cell Biology by Innovative Technology (Cell Innovation Program) from the MEXT to YH, and grant for the Genome Network Project from MEXT to YH. The funders had no role in study design, data collection and analysis, decision to publish, or preparation of the manuscript.

Competing Interests: The authors have declared that no competing interests exist.

* E-mail: rgscerg@gsc.riken.jp

☯ These authors contributed equally to this work.

Introduction

MicroRNA (miRNA) and small interfering RNA (siRNA) are small RNA approximately ~23 nucleotides in length which influence gene expression through post-transcriptional regulation of complementary target mRNA in the cytoplasm [1]. miRNA has also been linked to transcriptional silencing and heterochromatin formation in the nucleus [2] though the mechanistic details of these processes remain unclear, particularly in mammals.

DICER, widely conserved across eukaryotic lineages, is a member of the RNase III family of endoribonucleases and targets precursor miRNA (pre-miRNA) or long double-stranded RNA (dsRNA) to produce miRNA or siRNA as part of its essential role in various RNA interference (RNAi) pathways [3,4]. In mammals, the fundamental role of DICER in the RNAi pathway is thought to explain its linkage to a wide range of developmental processes including early development [5], centromeric silencing in embryonic stem (ES) cells [6], oocyte maturation [7,8], stem cell proliferation [9], and differentiation of many tissues [10,11,12].

The *Schizosaccharomyces pombe* DICER1 ortholog Dcr1 primarily accumulates in the nucleus and is associated with the nuclear pore complex at the nuclear periphery [13]. In the nucleus, Dcr1 associates with chromatin independent of the local level of transcriptional activity [14]. In humans, however, the initial discovery linking DICER1 to cytoplasmic RNAi and the subsequent detailed characterization of its functional role in this pathway [15,16,17] has led to the prevailing notion that the DICER1 protein is present solely in the cytoplasm [18,19,20]. However, several recent lines of investigation have questioned this assumption. First, evidence linking core RNAi components to heterochromatin formation in mammals have been provided by several reports [6,21]. Second, it has been shown that Dicer-deficient mouse embryonic stem (ES) cells are defective in the maintenance of centromeric heterochromatin structure and centromeric silencing [6]. Third, the DICER1 protein is known to regulate the transcription of an intergenic region of the human and chicken β-globin gene cluster [22,23]. Finally, human DICER1 associates with ribosomal DNA chromatin on the mitotic chromosomes [24]. Combination of the above observations suggested to us that human DICER1 protein might also localize and function in the nucleus.

Most nuclear proteins are transported into the nucleus through the nuclear pore complex (NPC), a structure comprised of ~30 different proteins known as nucleoporins (NUPs) which functions as a nuclear "gate" regulating the transport of macromolecules like proteins and nucleic acids across the nuclear membrane [25,26], via interaction with importin family proteins which often recognize specific amino acid sequences in the imported protein known as Nuclear Localization Signals (NLS). The importin-α family of nucleocytoplasmic shuttling proteins bind with NLS-containing proteins and transport the proteins into the nucleus with the assistance of an importin-β family protein [27]. Some proteins are shuttled independent of importin-α, relying exclusively on importin-β. For example, the importin-β family protein, transportin-1 (TNPO1) binds with proteins containing dsRNA-binding domains (dsRBDs) and transports these proteins into the nucleus

[28]. Interestingly, several NUPs of the NPC, long thought to act as passive structural components, were recently reported to have active transporter-like roles involving the binding of nucleus-targeted proteins and the shuttling of these proteins to the NPC for subsequent transport across the membrane [29,30,31,32]. This NUP-based transport is representative of several recent reports describing importin-independent nuclear transport pathways [27,33,34,35]. Given that human DICER1 appears to lack a canonical NLS for nuclear localization, we further reasoned that nuclear transport could be mediated by such non-canonical transport mechanisms that are just beginning to be understood.

We demonstrate here that human DICER1 protein is localized mainly in the cytoplasm but is also clearly present in the nucleoplasm. Further, we find that human DICER1 protein associates with the NUP153 protein in the cytoplasm and also at the nuclear periphery. On the basis of our results, we propose that NUP153 protein assists the DICER1 protein during transport and localization to the nucleus.

Results

Nuclear localization of human DICER1 protein

To investigate the possibility of nuclear localization of human DICER1 protein, Western blot analysis was performed using the cytoplasmic and nuclear extracts fractionated from 293T and HeLa cells (**Fig. 1A**). Distinctive DICER1 bands were detected on the lanes loaded not only in the cytoplasmic extract but also the nuclear extract. To determine if DICER1 protein was actually present inside the nucleus instead of being present at the surface of the nuclear membrane, we treated isolated nuclei from 293T cells with protease K and performed a Western blot analysis (**Fig. 1B**). The signals of NUP214 and NUP153 proteins, located on the periphery of nuclear pore complex, decreased after treatment

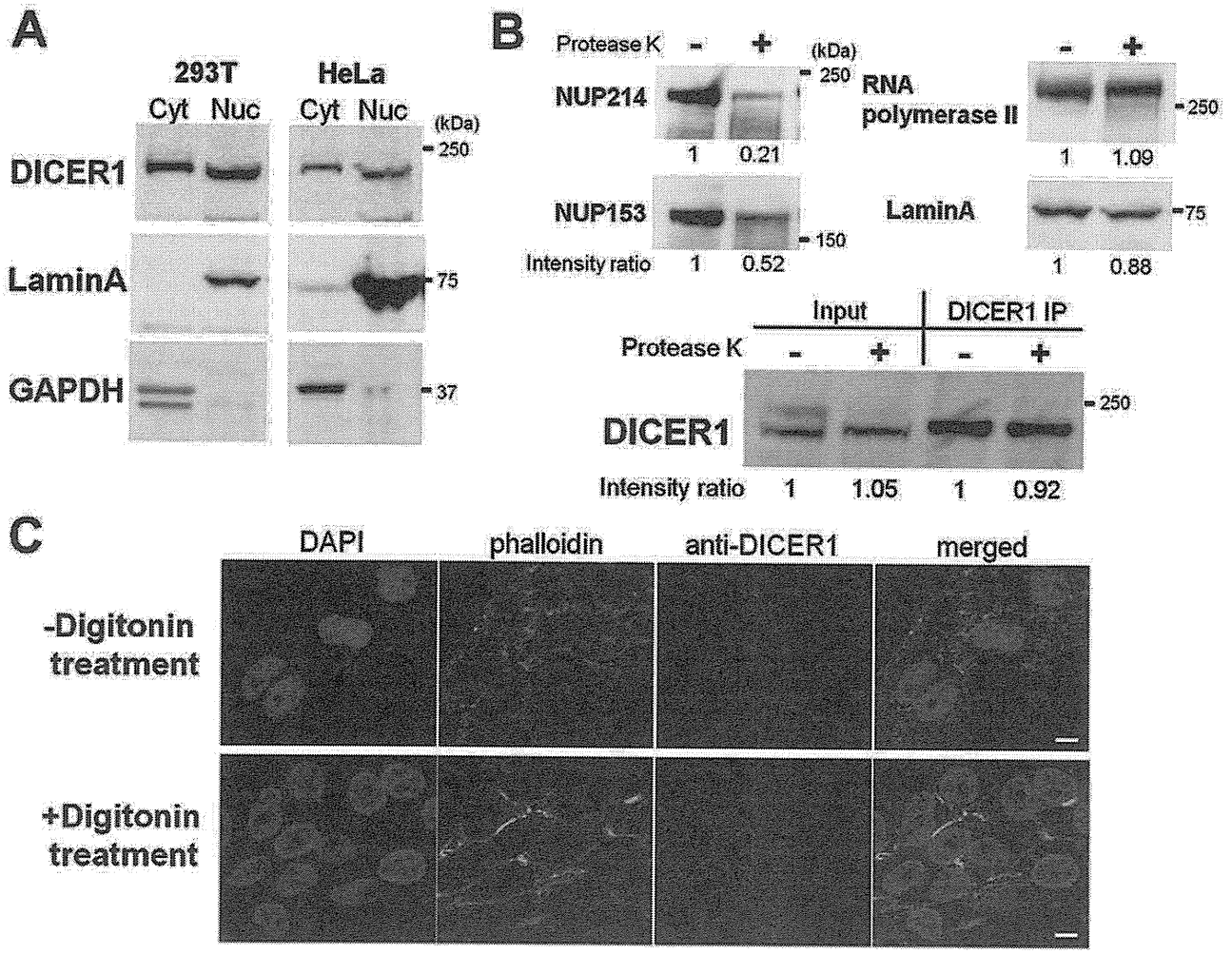

Figure 1. Nuclear localization of human DICER1 protein. (**A**) Western blot analysis for either cytoplasmic (Cyt) or nuclear (Nuc) extracts from 293T and HeLa cells using anti-DICER1, anti-LaminA and anti-GAPDH antibodies. LaminA and GAPDH were used as a nuclear or cytoplasmic marker protein, respectively. Each lane was loaded 50 μg of cytoplasmic extract or 100 μg of nuclear extract, respectively. (**B**) Western blot analysis for isolated nucleus with (+) or without (−) protease K treatment using anti-NUP214, anti-NUP153, anti-RNA polymerase II, anti-LaminA and anti-DICER1 antibodies. The signal intensity of each band was quantified using ImageJ software and intensity ratios were calculated from the "+" sample relative to the "−" sample. "Input" means the sample on 5% of volume used for immunoprecipitation (IP). (**C**) Confocal immunofluorescence images of DICER1 protein in HeLa cells without or with digitonin treatment. The signals of DICER1 protein (red) were detected using anti-DICER1 (12B5/4C6) antibody. Nuclei were counterstained with DAPI (blue) and cytoplasmic regions were co-stained with phalloidin (green). Scale bar represents 10 μm.
doi:10.1371/journal.pone.0023385.g001

while the signals of the RNA polymerase II and LaminA proteins, located in the nucleus, remained about the same. In this condition, the signal of DICER1 protein did not change after protease K treatment (**Fig. 1B**, input). These results were confirmed by immunoprecipitation of the same samples using the anti-DICER1 antibody (**Fig. 1B**, DICER1 IP). These results showed that human DICER1 protein localizes to the inside of the nucleus.

To further confirm the localization of DICER1 protein in the human cells, HeLa cells were immunostained with anti-DICER1 antibody. The confocal image in **Figure 1C (−digitonin treatment)** showed that most DICER1 protein signals, shown as red dots, were located in the cytoplasm but several signals overlapped with DAPI staining (blue colored). It was difficult to distinguish whether these signals were in the nucleoplasm or on the surface of the nucleus. Therefore, we permeabilized HeLa cells by digitonin treatment, washed out the cytoplasm and followed by immunofluorescence analysis using anti-DICER1 antibody (**Fig. 1C, +digitonin treatment**). Treatment of digitonin in appropriate concentration to the cells increases the permeability of the plasma membrane to cytoplasmic proteins without causing permeabilization of the nuclear membrane. The confocal image showed that DICER1 protein signals remained in the nucleus after digitonin treatment (**Fig. 1C, +digitonin treatment**). This supports localization of the DICER1 protein to the nucleoplasm, consistent with the result in **Figure 1B**. Our data demonstrated that human DICER1 protein is located in both the cytoplasm and nucleoplasm.

Identification of nucleoporins as DICER1-associated proteins

As human DICER1 protein lacks a canonical NLS for nuclear localization via interaction of importin-α proteins, this suggested nuclear DICER1 protein could be imported by a non-canonical transport system. In order to identify novel nuclear transport factors associated with human DICER1 protein, we co-immunoprecipitated DICER1-associated proteins using anti-DICER1 antibody from the cytoplasmic extract of 293T cells transiently expressing His-DICER1. TARBP2 (TRBP) [36,37] and PRKRA (PACT) [38] proteins, known as DICER1-associated proteins, co-immunoprecipitated with DICER1 protein (**Fig. 2**). The proteins were compared with the co-immunoprecipitated proteins from native 293T cells using the same antibody and the changed bands were analyzed using mass spectrometry (MS) (**Table S1**). We could detect four known DICER1-associated proteins (AGO2 [39], KHSRP [40], FMR1 [41] and TRBP [36,37]) (**Table 1**) as well as several interesting RNA-binding proteins like PUM1 and PUM2 [42,43], but failed to detect PACT and any importin family proteins in the MS results (**Table S1**).

Five NPC proteins (NUP214, NUP153, NUP98, NUP88 and SEC13), previously implicated in nucleocytoplasmic shuttling [29,30,31,32], were detected as candidate interacting proteins (**Table 1**). In particular, the NUP153 protein has been described as a highly mobile nucleoporin [44,45,46,47] which interacts directly with canonical nuclear import factors (**Fig. 3**). We focused our efforts on characterizing the extent of NUP153 protein interaction with the DICER1 protein due to the possibility of the NUP153 protein assisting in nuclear transport and also because the Mascot score [48] of the NUP153 protein was among the highest observed in the MS analysis (**Table 1**).

DICER1 protein interacts with NUP153 protein in HeLa cells

To validate the DICER1-NUP153 association, we performed co-immunoprecipitation with anti-DICER1 antibody using whole cell extract from 293T cells. Anti-DICER1 antibody immunoprecipitated with endogenous NUP153 protein, but mouse normal IgG did not (**Fig. 4A**). The co-immunoprecipitation experiments with anti-His antibody were performed using whole cell extract from 293T cells overexpressing His-DICER1 and NUP153 protein was detected in the co-immunoprecipitates (data not shown).

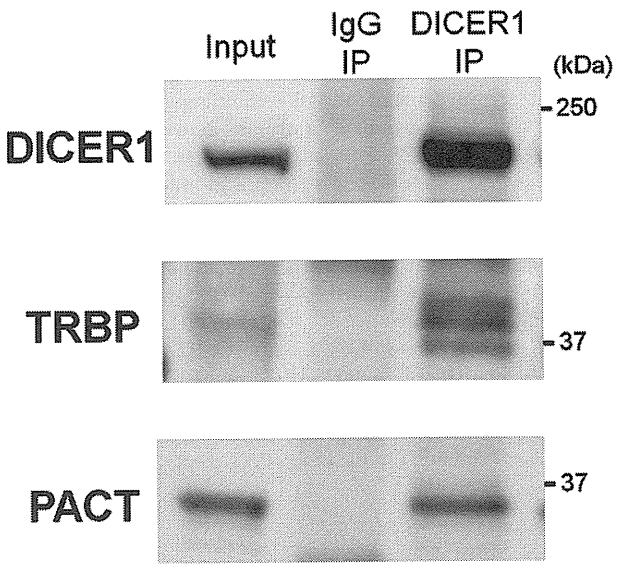

Figure 2. Co-immunoprecipitation (co-IP) of known DICER1-associated proteins with DICER1 protein in HeLa cells. Co-IP experiments using anti-DICER1 (12B5/4C6) antibody from HeLa total cell extracts followed by Western blot analysis with indicated antibodies. "Input" means the sample on 5% of volume used for IP.
doi:10.1371/journal.pone.0023385.g002

To investigate the association between DICER1 and NUP153 proteins in the cell, an *in situ* Proximity Ligation Assay (PLA) was performed. PLA is a method to detect protein-protein interactions with highly selectivity and sensitivity [49]. Briefly, in PLA, if two modified antibodies binding their respective epitopes are in sufficiently close proximity (typically less than 40 nm), this interaction is detected through emission of a red PLA signal. The PLA signals of DICER1-NUP153 association were detected mainly in the cytoplasm and partly at the nuclear periphery (**Fig. 4B** and **Movie S1**). In contrast, most signals of NUP153-LaminA association were detected only around the nuclear periphery, specifically localizing just inside of the nuclear membrane (**Fig. 4C** and **Movie S2**). No signal was observed in the absence of primary antibodies (**Fig. 4D** and **Movie S3**). This result indicated that DICER1 proteins associate with mobile NUP153 proteins in the cytoplasm, a fraction of DICER1 proteins associated with the NUP153 protein on the periphery of the NPC, and DICER1-NUP153 association was not observed in the nucleoplasm. This suggested that cytoplasmic association with NUP153 protein is meaningful for DICER1 protein and the cytoplasmic NUP153 protein may function in shuttling DICER1 protein to the NPC.

The NUP153 protein contributes to nuclear import of the DICER1 protein

To better characterize the involvement of NUP153 protein in nuclear transport of the DICER1 protein, a knockdown experiment was performed using siRNA for the NUP153 gene. Knockdown efficiency of the NUP153 gene was achieved at an 80% level, as determined by quantitative real-time PCR (qRT-PCR) averaging over three independent experiments (data not

Table 1. Proteins associated with human DICER1 protein.

Gene ID	Gene name	Synonym	Mw	Number of identified peptides	Mascot Score
Known components of pre-miRNA processing complex					
23405	DICER1	Endoribonuclease Dicer	217,490	88	2,223
27161	EIF2C2 (AGO2)	Protein argonaute-2	97,146	4	18
8570	KHSRP (KSRP)	Far upstream element-binding protein 2	73,101	2	43
2332	FMR1	Fragile X mental retardation 1 protein	71,131	3	41
6895	TARBP2 (TRBP)	RISC-loading complex subunit TARBP2	39,015	5	85
Nuclear pore complex proteins					
8021	NUP214	Nuclear pore complex protein Nup214	213,488	7	78
9972	NUP153	Nuclear pore complex protein Nup153	153,843	35	650
4928	NUP98	Nuclear pore complex protein Nup98-Nup96	187,673	3	29
4927	NUP88	Nuclear pore complex protein Nup88	83,489	1	31
6396	SEC13	Protein SEC13 homolog	35,518	2	54

doi:10.1371/journal.pone.0023385.t001

shown). This was confirmed by Western blot analysis of HeLa cell extracts using an anti-NUP153 antibody (**Fig. 5A**). The intensity ratio (Nuc/Cyt) of the DICER1 protein was significantly reduced in NUP153 knockdown (KD) samples compared to negative control (NC) samples transfected with NC siRNA (**Fig. 5B**). Meanwhile, the signals of LaminA and GAPDH proteins were not affected by NUP153 KD (**Fig. 5A**). Furthermore, immunofluorescence analysis was performed using human fibroblasts transfected with NC and NUP153 siRNAs (**Fig. 5C**). These results suggest that the NUP153 protein at least partially contributes to DICER1 protein import into the nucleus from the cytoplasm.

A recent report described nuclear import of the human ADAR1 protein via the importin-β-like TNPO1 protein which recognizes and interacts with a dsRBD of ADAR1 [28]. As human DICER1 also contains a dsRBD, we tested the potential role of TNPO1 in possibly supplementing the proposed NUP153-mediated transport. Western blot analysis was performed using co-immunoprecipitated samples with the DICER1 protein. No signal was detected between TNPO1 and DICER1 protein (**Fig. S1**). Interestingly, we similarly tested interaction with the importin-β1 (KPNB1) protein which is linked to importin-α-mediated nuclear transport and detected a very weak signal (**Fig. S1**). This data indicates that while DICER1 is not likely involved in TNPO1-mediated transport, some importin-β family members could contribute to nuclear transport, possibly in conjunction with NUP153.

Discussion

We demonstrate that DICER1 protein localizes not only to the cytoplasm but, like its counterparts in RNAi, the AGO-like proteins, DICER1 is also found in the nucleoplasm of human cells. This finding has the potential to expand the research fields

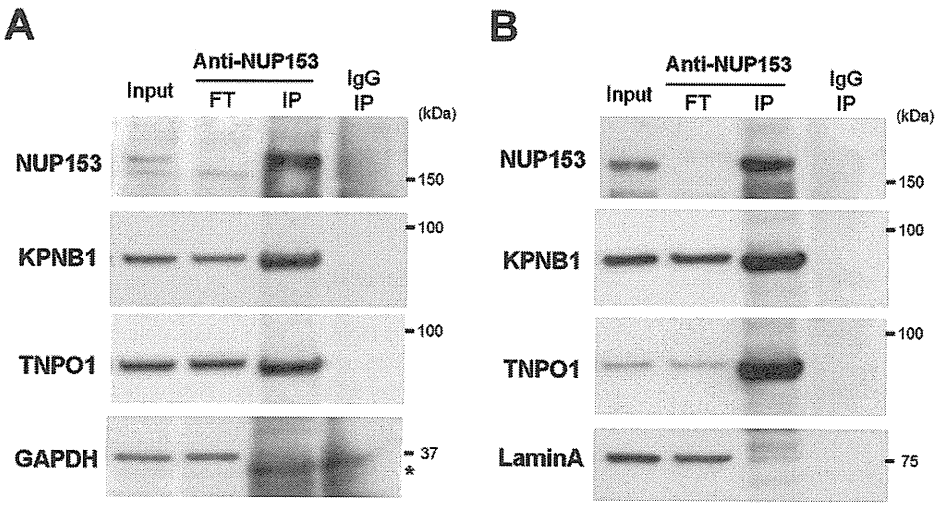

Figure 3. Co-IP of nuclear import receptor proteins with NUP153 protein. (**A**) Co-IP experiments with NUP153 protein from cytoplasmic extracts of HeLa cells followed by Western blot analysis with indicated antibodies. "Input" means the sample on 5% of volume used for IP and "FT" indicates the samples on 5% of flow-through solution of IP samples. The asterisk shows the non-specific band using anti-GAPDH antibody. (**B**) Co-IP with NUP153 protein from nuclear extracts of HeLa cells followed by Western blot analysis with indicated antibodies.
doi:10.1371/journal.pone.0023385.g003

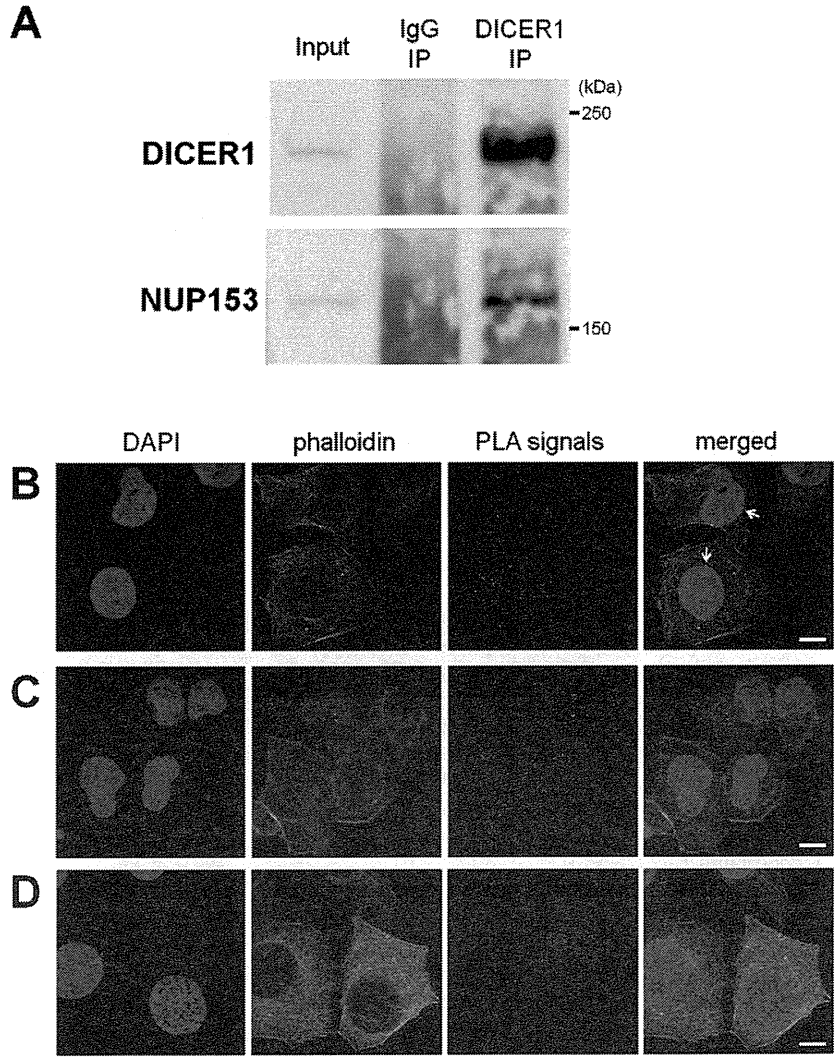

Figure 4. Association of NUP153 protein with DICER1 protein in HeLa cells. (**A**) Co-IP experiments from total cell extracts of HeLa cells followed by Western blot analysis with indicated antibodies. Endogenous NUP153 proteins were immunoprecipitated using anti-DICER1 antibody but not using mouse normal IgG (control). "Input" means the sample on 5% of volume used for IP. (**B**) *In situ* protein-protein associations between DICER1 and NUP153 were detected by Proximity Ligation Assay (PLA). HeLa cells were stained with mouse monoclonal anti-DICER1 and rabbit polyclonal anti-NUP153 antibodies and performed PLA. The association signals were detected by Duolink 100 Detection Kit 613 (red), and nuclei were counterstained with DAPI (blue). Samples co-stained with phalloidin (green) allow visualization of cell borders. Each red dot represents the detection of protein-protein association complex. White arrows indicate the signals at the nuclear periphery. Scale bar represents 10 μm. (**C**) PLA image shows the protein-protein associations between NUP153 and LaminA inside of nuclear membrane. (**D**) A negative control experiment of PLA was performed without addition of any primary antibodies.
doi:10.1371/journal.pone.0023385.g004

relating to a small RNA in the nucleus, including its mechanism of biogenesis. In murine cells, pre-mmu-mir-1982 RNA, which is a mirtron with an 11 nt tail at the 5′ end, is spliced out [50]. This unusual pre-miRNA structure is not compatible with nuclear export by Exportin-5 [51]. Despite this, miR-1982* miRNA emerges without 11 nt-5′ overhangs from the deep sequencing data of murine cells [50,52]. We recently reported that human DICER1 protein could process this pre-mmu-mir-1982 RNA to mature double-stranded miRNA without 5′ overhangs *in vitro* [53]. These observations suggest human DICER1 protein could function in the processing of small RNAs in the nucleus.

Several lines of very recent investigation also hint at other possible function roles for DICER1 in the nucleus. In fission yeast, it was recently reported that Dcr1 protein physically associates with chromatin and H3K9 methylation is not required for the association [14]. Sinkkonen *et al.* showed human DICER1 protein associates with ribosomal DNA loci via immunostaining of mitotic chromosomes [24]. Intriguingly, chromatin immunoprecipitation (ChIP)-seq data with anti-DICER1 (12B5/4C6) antibody suggests the DICER1 protein associates with specific DNA regions and most adjacent genes to the regions were transcribed (unpublished observations, Ando Y, *et al.*). The combination of the above observations together with the experimental data presented in this manuscript could suggest that human DICER1 proteins, while mainly localizing in the cytoplasm as an important component of the RNAi pathway, are also imported actively into the nucleus under the guidance of the NUP153 protein and ultimately associate with active regions of chromatin. Future work will be

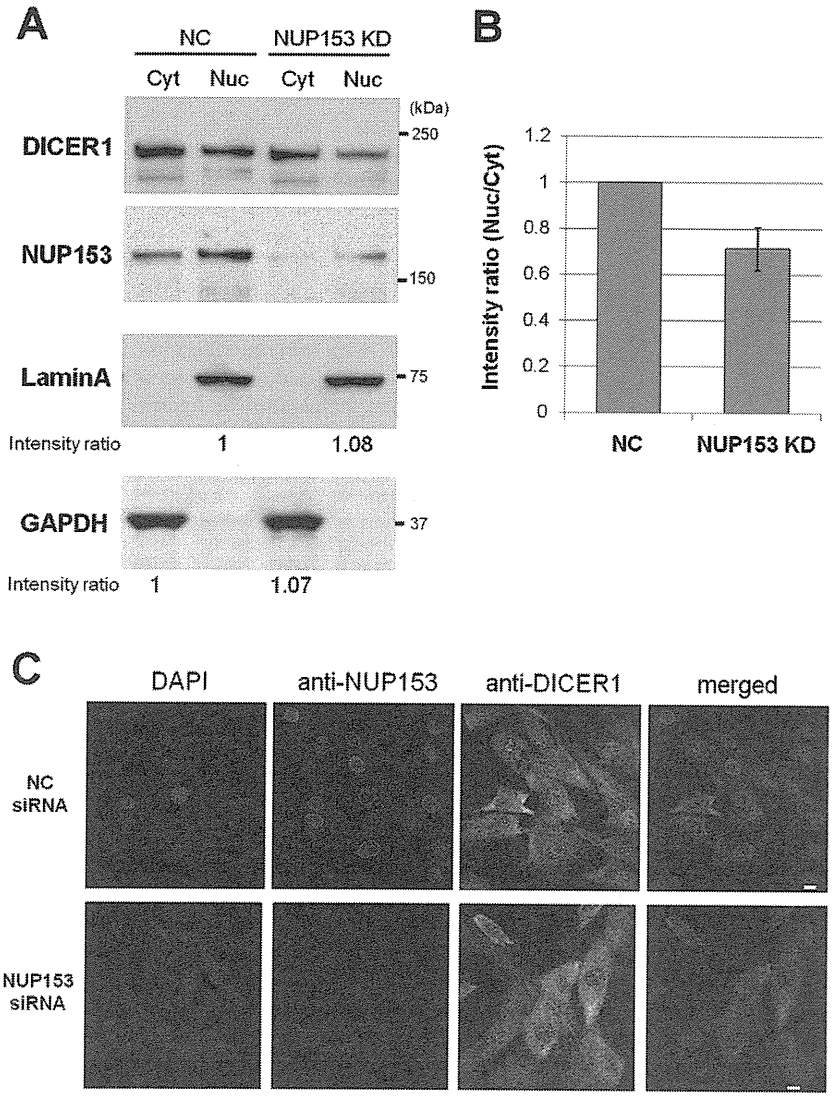

Figure 5. Effects of siRNA knockdown against NUP153. (**A**) Western blot analysis of negative control (NC) and NUP153 knockdown (KD) samples with indicated antibodies. Each lane was loaded 40 μg of cytoplasmic or nuclear extract, respectively. (**B**) Intensity ratio (Nuc/Cyt) of DICER1 protein in NUP153 KD sample is normalized to the intensity ratio of NC sample. The signal intensity of each band was quantified using ImageJ software. These plots show average values of the relative intensity ratio bracketed by s.e.m. error bars; calculated from three independent experiments. (**C**) Confocal immunofluorescence images in human fibroblasts transfected with NC or NUP153 siRNAs. The signals of NUP153 and DICER1 proteins were detected using rabbit polyclonal anti-NUP153 and mouse monoclonal anti-DICER1 antibodies, respectively. Nuclei were counterstained with DAPI. In merged figure, red, green and blue colors represent the signals of NUP153, DICER1 proteins and DAPI, respectively. Scale bar represents 10 μm.
doi:10.1371/journal.pone.0023385.g005

required to more clearly elucidate functions of human DICER1 protein in the nucleus.

In total, we identified 70 novel DICER1-associated protein candidates from cytoplasmic extract, shown in **Table S1**. In the list, we identified five nucleoporins (NUP214, NUP153, NUP98, NUP88 and SEC13) (**Table 1**). All of these proteins have a demonstrated ability in nucleocytoplasmic shuttling and function in the nucleocytoplasmic transport of macromolecules [29,30,31,32]. Our study links the import of human DICER1 protein with the NUP153 protein. However, it is very likely that another factor also contributes to nuclear import and we cannot rule out the possibility that a decrease of NUP153 protein as a structural component of the NPC may lead to a general decrease in nuclear transport.

We also identified 30 RNA-binding proteins, defined from Gene Ontology (http://geneontology.org/) analysis, and some RISC-associating proteins [54] associating with DICER1 in **Table S1**. Recently, it was reported that two RNA-binding proteins PUM1 and PUM2, identified as DICER1-associated protein candidates in this study, regulate miRNA-dependent gene silencing [42,43]. The binding of the PUM proteins to target mRNA induces a local conformational change in the 3′ UTR of target mRNA that exposes a specific miRNA-binding site [42]. The DICER1 protein may mediate this regulation via its associations with RNA-binding proteins and RISC-associating proteins.

In summary, these findings have wide-ranging implications for the functional role and interacting partners of human DICER1.

We also provide the first possible mode of molecular import via interaction with the nuclear shuttling factor, NUP153.

Materials and Methods

Antibodies

Mouse monoclonal anti-hDICER1 (12B5/4C6) was raised in house by using full-length human DICER1 protein as antigens. Rabbit polyclonal anti-hDICER1 (H212, SantaCruz, sc-30226), rabbit polyclonal anti-hTRBP (Abcam, ab42018), rabbit polyclonal anti-hNUP153 (Abcam, ab84872), mouse monoclonal anti-hNUP153 (QE5, Abcam, ab24700), rabbit polyclonal anti-hNUP214 (Abcam, ab70497), mouse monoclonal anti-hLaminA (133A2, Abcam, ab8980), rabbit polyclonal anti-hLaminA (Abcam, ab2559), goat polyclonal anti-hGAPDH (I-19, SantaCruz, sc-48166), mouse monoclonal anti-RNA polymerase II CTD repeat YSPTSPS (4H8, Abcam, ab5408), mouse monoclonal anti-hKPNB1 (31H4, Sigma, I2534) and mouse monoclonal anti-hTNPO1 (D45, Sigma, T0825) were used as primary antibody for Western blotting and immunofluorescence. Mouse Normal IgG (Millipore, 12-371) was used as a control for immunoprecipitation. Alexa flour 488 Donkey anti-rabbit IgG(H+L) (Molecular probe, A11055), Alexa flour 488 Donkey anti-mouse IgG(H+L) (Molecular probe, A21202), Alexa flour 594 Donkey anti-rabbit IgG(H+L) (Molecular probe A21207) and Alexa flour 594 Donkey anti-rabbit IgG(H+L) (Molecular probe A21203) were used as secondary antibody for immunofluorescence. Phalloidin Alexa flour 488 (Molecular probe A12379) and DAPI was used for cytoplasmic and nuclear staining, respectively.

Cell culture, cytoplasmic and nuclear protein extraction

The 293T and HeLa cells were cultured in DMEM (Invitrogen, 11885) and 10% FBS in a 5% CO_2 at 37°C. The human normal skin fibroblast cells (NB1RGB), which were established in RIKEN BioResource Center from male 3days old neonate, were cultured in MEM alpha (Wako, 135-15175) supplemented with 10% FBS and Penicillin/Streptomycin (Invitrogen) in a 5% CO_2 at 37°C. All cell lines were purchased from RIKEN BioResource Center.

Cultured cells were collected, washed twice with cold PBS and incubated in SolutionA (50 mM Tris-HCl pH 7.5, 0.8 M Sucrose, 150 mM Potassium chloride, 5 mM Magnesium chloride, 6 mM β-mercaptoethanol, 0.5% NP-40 and protease inhibitor) for 10 min on ice [55]. Cytoplasmic extracts were cleared by centrifugation at 16,000×g for 15 min at 4°C. Pellets were washed twice with SolutionA (isolated nucleus) and suspended with RIPA buffer by vortexing and sonication. Nuclear extracts were cleared by centrifugation at 16,000×g for 15 min at 4°C. The extracts were quantified using a Protein Assay Kit (Biorad). Isolated nuclei were treated with 2 ng/μl protease K (Invitrogen) in PBS for 5 min at 37°C, washed with PBS and suspended with RIPA buffer by vortexing and sonication.

Western blot analysis

The protein samples were separated by 4–12% NuPAGE Bis-Tris Gel (Invitrogen) and transferred to the PVDF membrane (Millipore). Detection was achieved with primary antibodies described above and peroxidase-conjugated anti-rabbit (GE Healthcare), anti-mouse (GE Healthcare) and anti-goat (Biorad) antibodies were used as secondary antibodies. The signal intensity of each band was quantified with ImageJ software (http://rsbweb.nih.gov/ij/). The membrane was re-probed by different antibodies after removal of antibodies using Restore PLUS Western Blot Stripping Buffer (Thermo Scientific) from Western blots.

Cytoplasmic membrane permeabilization

Cells grown on Lab-tek chamber slide (Nunc, 177402) were washed two times with ice cold Transport Buffer (20 mM HEPES pH 7.3, 110 mM Potassium acetate, 5 mM Sodium acetate, 2 mM Magnesium acetate, 1 mM EGTA, 2 mM DTT and protease inhibitor). Washed cells were permeabilized with 40 μg/ml digitonin in Transport buffer for 5 min on ice. Permiabilized cells were preceded to immunoflorescence after washing twice with Transport Buffer and washing twice with PBS [56].

Immunofluorescence and Proximity Ligation Assay

The procedure for immunofluorescence was essentially as previously described [57] with some modification. Cells grown on Lab-tek chamber slide were fixed with 4% paraformaldehyde in PBS for 10 min at room temperature and permeabilized with 0.5% Triton X-100 in PBS for 4 min at room temperature. The chambers were subsequently incubated for blocking with Blocking One (Nacalai, 03953-95) for 30 min at 37°C. After blocking, cells on chamber were incubated with Blocking One and diluted primary antibody for 45 min at 37°C. After primary antibody incubation, cells were washed with PBS three times and incubated with Blocking One, diluted secondary antibody and phalloidin for 45 min at 37°C. Cells were subsequently washed with PBS three times and mounted with Vectashield with DAPI (Vector laboratories, HT-1200). The Proximity Ligation Assay was performed with DuoLink system (O-link) according to the manufacturer's instructions. Immunofluorescence and proximity ligation assay samples were observed and photographed at 63× magnifications under a confocal laser scanning microscopy system (Leica).

cDNA cloning and construction of plasmid

We assembled a full-length cDNA of human DICER1 protein from HeLa total RNA. This cDNA sequence was identical to the coding sequence cited in the Swiss-Prot Protein Database (http://au.expasy.org/sprot/) [Swiss-Prot: Q9UPY3]. The cDNA was cloned in a pDEST26 vector (Invitrogen). N-terminally His-tagged human DICER1 protein (His-DICER1) was expressed in 293T cells transfected with the plasmid pDEST26-DICER1.

Co-immunoprecipitation

Co-immunoprecipitation of DICER1-associated proteins was performed using anti-DICER1 (12B5/4C6) antibody and Dynabeads Protein G (Invitrogen) according to manufacturer's instructions. Each immunoprecipitated protein was detected by Western blot analysis to check for successful co-IP using anti-DICER1, anti-TRBP and anti-PACT antibodies. For the co-immunoprecipitation experiments with NUP153 proteins, anti-NUP153 (QE5) antibody was used. Mouse Normal IgG (Millipore) was used as a control for co-immunoprecipitation. Tenty-five μl of Dynabeads Protein G was mixed with 2.5 μg of the antibody. Then, 200 μg of each cytoplasmic and nuclear extracts in 150 μl B&W buffer (0.1 M sodium phosphate buffer pH 8.2, 0.01% Tween20) was added to the beads-antibody complex and mixed by rotation for 2 hours at 4°C. Supernatants were used as a flowthrough fraction. Beads were washed four times with B&W buffer, and each bound complex was eluted by adding 20 μl of premixed NuPAGE LDS Sample Buffer (Invitrogen) and NuPAGE Sample Reducing Agent (Invitrogen). Immunoprecipitated proteins were separated by NuPAGE Novex 4–12% Bis-Tris gel for Western blot analysis and 10% SDS-PAGE gel for MS analysis.

Identification of proteins by MS

Protein bands were excised from gels stained by Silver Stain MS Kit (Wako), and in-gel digestion was performed as previously described [58]. Briefly, the gel pieces were washed three times with 60% acetonitrile that contained 50 mM NH_4HCO_3, and then dried completely. The dried gel pieces were incubated with 50 mM NH_4HCO_3 that contained 25 ng/μl trypsin (Trypsin Gold, MS Grade; Promega) for 16 hours at 37°C. After digestion, 1 μl of formic acid was added to the buffer to stop the reaction. The peptide fragments were desalted and concentrated with ZipTip (Millipore), then eluted with 80% acetonitrile and 0.1% formic acid. The samples were dried completely and solved with 10 μl of formic acid, then injected into LC/LIT-TOF MS (NanoFrontier eLD, Hitachi High-Tech). The peptide mass fingerprints were analyzed using the MASCOT search program (Matrix Science, http://www.matrixscience.com), searching the Swiss-prot database (http://au.expasy.org/sprot/). The quality of peptide product ion spectra is shown as a Mascot score [48].

siRNA transfection and RNA extraction

Stealth siRNA for NUP153 (5′-UGGGAGUGUUCAGUAUGCUGUGUUU-3′) and NC siRNA (Stealth RNAi Negative Control Medium GC Duplex #2) were purchased from Invitrogen. Transfections of siRNA were performed with Lipofectamin RNAiMAX (Invitorogen) in Opti-MEM medium (Invitrogen) according to the manfacturer's instruction. Total RNAs were extracted 48 hours after transfection with TRIzol (Invitrogen) and FastPure RNA kit (Takara Bio) as previously described [59]. RNA was quantified with NanoDrop (NanoDrop Technologies).

qRT-PCR for mRNA expression analysis

Expression levels of gene in the gene specific siRNAs or the calibrator negative control siRNA transfected cells were estimated by qRT-PCR with gene specific primer pairs. Reverse transcription reaction was performed with PrimeScript RT-PCR Kit (Perfect Real Time, Takara Bio) according to the manufacturer's instructions. qRT-PCR was performed in 10 μl reaction mixture with SYBR Premix Ex Taq (Perfect Real Time, Takara Bio) on an ABI 7500 Fast Real-Time PCR system (Applied Biosystems). Details of procedure and condition were essentially same as previously described [60]. The primer sequences used for qRT-PCR in this study are NUP153-F: 5′-GGCGACAACAGCATCAGGGCA-3′ and NUP153-R: 5′-TCTGGCCAGCGTGGAACCTC-3′.

Supporting Information

Figure S1 Co-immunoprecipitation of nuclear import receptor proteins with DICER1 protein. Co-immunoprecipitation of DICER1 protein from cytoplasmic extracts of HeLa cells followed by Western blot analysis with indicated antibodies. "Input" means the sample on 5% of volume used for immunoprecipitation (IP) and "FT" indicates the samples on 5% of flow-through solution of IP samples. The asterisk shows the non-specific band using anti-GAPDH antibody.
(TIF)

Movie S1 Related to Figure 4B. Confocal image of PLA using mouse monoclonal anti-DICER1 (12B5/4C6) and rabbit polyclonal anti-NUP153 antibody.
(MOV)

Movie S2 Related to Figure 4C. Confocal image of PLA using mouse monoclonal anti-NUP153 and rabbit polyclonal anti-LaminA antibodies.
(MOV)

Movie S3 Related to Figure 4D. Confocal image of PLA without addition of any primary antibodies.
(MOV)

Table S1
(DOC)

Acknowledgments

We thank Drs. Timo Lassmann and Yuki Tanaka for their helpful discussion.

Author Contributions

Conceived and designed the experiments: YA HS PC YH. Performed the experiments: YA YT AM AK. Analyzed the data: AMB HK YI HH. Contributed reagents/materials/analysis tools: RK MT JC. Wrote the paper: YA AMB.

References

1. Ambros V (2004) The functions of animal microRNAs. Nature 431: 350–355.
2. Lippman Z, Martienssen R (2004) The role of RNA interference in heterochromatic silencing. Nature 431: 364–370.
3. Cerutti H, Casas-Mollano JA (2006) On the origin and functions of RNA-mediated silencing: from protists to man. Curr Genet 50: 81–99.
4. Muljo SA, Kanellopoulou C, Aravind L (2010) MicroRNA targeting in mammalian genomes: genes and mechanisms. Wiley Interdiscip Rev Syst Biol Med 2: 148–161.
5. Bernstein E, Kim SY, Carmell MA, Murchison EP, Alcorn H, et al. (2003) Dicer is essential for mouse development. Nat Genet 35: 215–217.
6. Kanellopoulou C, Muljo SA, Kung AL, Ganesan S, Drapkin R, et al. (2005) Dicer-deficient mouse embryonic stem cells are defective in differentiation and centromeric silencing. Genes Dev 19: 489–501.
7. Murchison EP, Stein P, Xuan Z, Pan H, Zhang MQ, et al. (2007) Critical roles for Dicer in the female germline. Genes Dev 21: 682–693.
8. Tang F, Kaneda M, O'Carroll D, Hajkova P, Barton SC, et al. (2007) Maternal microRNAs are essential for mouse zygotic development. Genes Dev 21: 644–648.
9. Murchison EP, Partridge JF, Tam OH, Cheloufi S, Hannon GJ (2005) Characterization of Dicer-deficient murine embryonic stem cells. Proc Natl Acad Sci U S A 102: 12135–12140.
10. Cuellar TL, Davis TH, Nelson PT, Loeb GB, Harfe BD, et al. (2008) Dicer loss in striatal neurons produces behavioral and neuroanatomical phenotypes in the absence of neurodegeneration. Proc Natl Acad Sci U S A 105: 5614–5619.
11. Koralov SB, Muljo SA, Galler GR, Krek A, Chakraborty T, et al. (2008) Dicer ablation affects antibody diversity and cell survival in the B lymphocyte lineage. Cell 132: 860–874.
12. Zehir A, Hua LL, Maska EL, Morikawa Y, Cserjesi P (2010) Dicer is required for survival of differentiating neural crest cells. Dev Biol 340: 459–467.
13. Emmerth S, Schober H, Gaidatzis D, Roloff T, Jacobeit K, et al. (2010) Nuclear retention of fission yeast dicer is a prerequisite for RNAi-mediated heterochromatin assembly. Dev Cell 18: 102–113.
14. Woolcock KJ, Gaidatzis D, Punga T, Buhler M (2011) Dicer associates with chromatin to repress genome activity in Schizosaccharomyces pombe. Nat Struct Mol Biol 18: 94–99.
15. Billy E, Brondani V, Zhang H, Muller U, Filipowicz W (2001) Specific interference with gene expression induced by long, double-stranded RNA in mouse embryonal teratocarcinoma cell lines. Proc Natl Acad Sci U S A 98: 14428–14433.
16. Provost P, Dishart D, Doucet J, Frendewey D, Samuelsson B, et al. (2002) Ribonuclease activity and RNA binding of recombinant human Dicer. EMBO J 21: 5864–5874.
17. Kotaja N, Bhattacharyya SN, Jaskiewicz L, Kimmins S, Parvinen M, et al. (2006) The chromatoid body of male germ cells: similarity with processing bodies and presence of Dicer and microRNA pathway components. Proc Natl Acad Sci U S A 103: 2647–2652.
18. Moser JJ, Eystathioy T, Chan EK, Fritzler MJ (2007) Markers of mRNA stabilization and degradation, and RNAi within astrocytoma GW bodies. J Neurosci Res 85: 3619–3631.

19. Daniels SM, Melendez-Pena CE, Scarborough RJ, Daher A, Christensen HS, et al. (2009) Characterization of the TRBP domain required for dicer interaction and function in RNA interference. BMC Mol Biol 10: 38.
20. Jakymiw A, Patel RS, Deming N, Bhattacharyya I, Shah P, et al. (2010) Overexpression of dicer as a result of reduced let-7 MicroRNA levels contributes to increased cell proliferation of oral cancer cells. Genes Chromosomes Cancer 49: 549–559.
21. Fukagawa T, Nogami M, Yoshikawa M, Ikeno M, Okazaki T, et al. (2004) Dicer is essential for formation of the heterochromatin structure in vertebrate cells. Nat Cell Biol 6: 784–791.
22. Haussecker D, Proudfoot NJ (2005) Dicer-dependent turnover of intergenic transcripts from the human beta-globin gene cluster. Mol Cell Biol 25: 9724–9733.
23. Giles KE, Ghirlando R, Felsenfeld G (2010) Maintenance of a constitutive heterochromatin domain in vertebrates by a Dicer-dependent mechanism. Nat Cell Biol 12: 94–99; sup pp 91–96.
24. Sinkkonen L, Hugenschmidt T, Filipowicz W, Svoboda P (2010) Dicer is associated with ribosomal DNA chromatin in mammalian cells. PLoS One 5: e12175.
25. Terry LJ, Shows EB, Wente SR (2007) Crossing the nuclear envelope: hierarchical regulation of nucleocytoplasmic transport. Science 318: 1412–1416.
26. Strambio-De-Castillia C, Niepel M, Rout MP (2010) The nuclear pore complex: bridging nuclear transport and gene regulation. Nat Rev Mol Cell Biol 11: 490–501.
27. Wagstaff KM, Jans DA (2009) Importins and beyond: non-conventional nuclear transport mechanisms. Traffic 10: 1188–1198.
28. Fritz J, Strehblow A, Taschner A, Schopoff S, Pasierbek P, et al. (2009) RNA-regulated interaction of transportin-1 and exportin-5 with the double-stranded RNA-binding domain regulates nucleocytoplasmic shuttling of ADAR1. Mol Cell Biol 29: 1487–1497.
29. Marg A, Shan Y, Meyer T, Meissner T, Brandenburg M, et al. (2004) Nucleocytoplasmic shuttling by nucleoporins Nup153 and Nup214 and CRM1-dependent nuclear export control the subcellular distribution of latent Stat1. J Cell Biol 165: 823–833.
30. Griffis ER, Xu S, Powers MA (2003) Nup98 localizes to both nuclear and cytoplasmic sides of the nuclear pore and binds to two distinct nucleoporin subcomplexes. Mol Biol Cell 14: 600–610.
31. Takahashi N, van Kilsdonk JW, Ostendorf B, Smeets R, Bruggeman SW, et al. (2008) Tumor marker nucleoporin 88 kDa regulates nucleocytoplasmic transport of NF-kappaB. Biochem Biophys Res Commun 374: 424–430.
32. Enninga J, Levay A, Fontoura BM (2003) Sec13 shuttles between the nucleus and the cytoplasm and stably interacts with Nup96 at the nuclear pore complex. Mol Cell Biol 23: 7271–7284.
33. Xu L, Alarcon C, Col S, Massague J (2003) Distinct domain utilization by Smad3 and Smad4 for nucleoporin interaction and nuclear import. J Biol Chem 278: 42569–42577.
34. Asally M, Yoneda Y (2005) Beta-catenin can act as a nuclear import receptor for its partner transcription factor, lymphocyte enhancer factor-1 (lef-1). Exp Cell Res 308: 357–363.
35. Zhong H, Takeda A, Nazari R, Shio H, Blobel G, et al. (2005) Carrier-independent nuclear import of the transcription factor PU.1 via RanGTP-stimulated binding to Nup153. J Biol Chem 280: 10675–10682.
36. Chendrimada TP, Gregory RI, Kumaraswamy E, Norman J, Cooch N, et al. (2005) TRBP recruits the Dicer complex to Ago2 for microRNA processing and gene silencing. Nature 436: 740–744.
37. Haase AD, Jaskiewicz L, Zhang H, Laine S, Sack R, et al. (2005) TRBP, a regulator of cellular PKR and HIV-1 virus expression, interacts with Dicer and functions in RNA silencing. EMBO Rep 6: 961–967.
38. Lee Y, Hur I, Park SY, Kim YK, Suh MR, et al. (2006) The role of PACT in the RNA silencing pathway. EMBO J 25: 522–532.
39. Tahbaz N, Kolb FA, Zhang H, Jaronczyk K, Filipowicz W, et al. (2004) Characterization of the interactions between mammalian PAZ PIWI domain proteins and Dicer. EMBO Rep 5: 189–194.
40. Trabucchi M, Briata P, Garcia-Mayoral M, Haase AD, Filipowicz W, et al. (2009) The RNA-binding protein KSRP promotes the biogenesis of a subset of microRNAs. Nature 459: 1010–1014.
41. Jin P, Zarnescu DC, Ceman S, Nakamoto M, Mowrey J, et al. (2004) Biochemical and genetic interaction between the fragile X mental retardation protein and the microRNA pathway. Nat Neurosci 7: 113–117.
42. Kedde M, van Kouwenhove M, Zwart W, Oude Vrielink JA, Elkon R, et al. (2010) A Pumilio-induced RNA structure switch in p27-3′ UTR controls miR-221 and miR-222 accessibility. Nat Cell Biol 12: 1014–1020.
43. Leibovich L, Mandel-Gutfreund Y, Yakhini Z (2010) A structural-based statistical approach suggests a cooperative activity of PUM1 and miR-410 in human 3′-untranslated regions. Silence 1: 17.
44. Daigle N, Beaudouin J, Hartnell L, Imreh G, Hallberg E, et al. (2001) Nuclear pore complexes form immobile networks and have a very low turnover in live mammalian cells. J Cell Biol 154: 71–84.
45. Rabut G, Doye V, Ellenberg J (2004) Mapping the dynamic organization of the nuclear pore complex inside single living cells. Nat Cell Biol 6: 1114–1121.
46. Rabut G, Lenart P, Ellenberg J (2004) Dynamics of nuclear pore complex organization through the cell cycle. Curr Opin Cell Biol 16: 314–321.
47. Ball JR, Ullman KS (2005) Versatility at the nuclear pore complex: lessons learned from the nucleoporin Nup153. Chromosoma 114: 319–330.
48. Koenig T, Menze BH, Kirchner M, Monigatti F, Parker KC, et al. (2008) Robust prediction of the MASCOT score for an improved quality assessment in mass spectrometric proteomics. J Proteome Res 7: 3708–3717.
49. Soderberg O, Gullberg M, Jarvius M, Ridderstrale K, Leuchowius KJ, et al. (2006) Direct observation of individual endogenous protein complexes in situ by proximity ligation. Nat Methods 3: 995–1000.
50. Berezikov E, Chung WJ, Willis J, Cuppen E, Lai EC (2007) Mammalian mirtron genes. Mol Cell 28: 328–336.
51. Okada C, Yamashita E, Lee SJ, Shibata S, Katahira J, et al. (2009) A high-resolution structure of the pre-microRNA nuclear export machinery. Science 326: 1275–1279.
52. Chiang HR, Schoenfeld LW, Ruby JG, Auyeung VC, Spies N, et al. (2010) Mammalian microRNAs: experimental evaluation of novel and previously annotated genes. Genes Dev 24: 992–1009.
53. Ando Y, Maida Y, Morinaga A, Burroughs AM, Kimura R, et al. (2011) Two-step cleavage of hairpin RNA with 5′ overhangs by human DICER. BMC Mol Biol 12.
54. Hock J, Weinmann L, Ender C, Rudel S, Kremmer E, et al. (2007) Proteomic and functional analysis of Argonaute-containing mRNA-protein complexes in human cells. EMBO Rep 8: 1052–1060.
55. Carninci P, Nakamura M, Sato K, Hayashizaki Y, Brownstein MJ (2002) Cytoplasmic RNA extraction from fresh and frozen mammalian tissues. Biotechniques 33: 306–309.
56. Adam SA, Marr RS, Gerace L (1990) Nuclear protein import in permeabilized mammalian cells requires soluble cytoplasmic factors. J Cell Biol 111: 807–816.
57. Jul-Larsen A, Visted T, Karlsen BO, Rinaldo CH, Bjerkvig R, et al. (2004) PML-nuclear bodies accumulate DNA in response to polyomavirus BK and simian virus 40 replication. Exp Cell Res 298: 58–73.
58. Intoh A, Kurisaki A, Yamanaka Y, Hirano H, Fukuda H, et al. (2009) Proteomic analysis of membrane proteins expressed specifically in pluripotent murine embryonic stem cells. Proteomics 9: 126–137.
59. Burroughs AM, Ando Y, de Hoon MJ, Tomaru Y, Nishibu T, et al. (2010) A comprehensive survey of 3′ animal miRNA modification events and a possible role for 3′ adenylation in modulating miRNA targeting effectiveness. Genome Res 20: 1398–1410.
60. Tomaru Y, Simon C, Forrest AR, Miura H, Kubosaki A, et al. (2009) Regulatory interdependence of myeloid transcription factors revealed by Matrix RNAi analysis. Genome Biol 10: R121.

Biochimica et Biophysica Acta 1814 (2011) 265–276

Contents lists available at ScienceDirect

Biochimica et Biophysica Acta

journal homepage: www.elsevier.com/locate/bbapap

Proteomic identification of differentially expressed genes in neural stem cells and neurons differentiated from embryonic stem cells of cynomolgus monkey (*Macaca fascicularis*) in vitro

Kuniko Akama [a,b,*], Tomoe Horikoshi [a], Takashi Nakayama [c], Masahiro Otsu [d,e], Noriaki Imaizumi [a], Megumi Nakamura [f], Tosifusa Toda [f], Michiko Inuma [g], Hisashi Hirano [h,g], Yasushi Kondo [i], Yutaka Suzuki [i], Nobuo Inoue [d]

[a] *Department of Chemistry, Graduate School of Science, Chiba University, Chiba, Japan*
[b] *Center for General Education, Chiba University, Chiba, Japan*
[c] *Department of Biochemistry, Yokohama City University School of Medicine, Yokohama, Japan*
[d] *Laboratory of Regenerative Neurosciences, Graduate School of Human Health Science, Tokyo Metropolitan University, Tokyo, Japan*
[e] *Department of Chemistry, Kyorin University, School of Medicine, Tokyo, Japan*
[f] *Proteome, Mechanism of Aging, Tokyo Metropolitan Institute of Gerontology, Tokyo, Japan*
[g] *Advanced Medical Research Center, Yokohama City University, Yokohama, Japan*
[h] *Department of Supramolecular Biology, Graduate School of Nanobioscience, Yokohama City University, Yokohama, Japan*
[i] *Regenerative Medicine, Advanced Medical Research Laboratory, Mitsubishi Tanabe Pharma Co, Osaka, Japan*

ARTICLE INFO

Article history:
Received 28 July 2010
Received in revised form 20 October 2010
Accepted 26 October 2010
Available online xxxx

Keywords:
Embryonic stem cells
Differential expression
Neural stem cells
Neuronal differentiation
Monkey

ABSTRACT

Understanding neurogenesis is valuable for the treatment of nervous system disorders. However, there is currently limited information about the molecular events associated with the transition from primate ES cells to neural cells. We therefore sought to identify the proteins involved in neurogenesis, from *Macaca fascicularis* ES cells (CMK6 cell line) to neural stem (NS) cells to neurons using two-dimensional gel electrophoresis (2-DE), peptide mass fingerprinting (PMF), and liquid chromatography-tandem mass spectrometry (LC-MS-MS). During the differentiation of highly homogeneous ES cells to NS cells, we identified 17 proteins with increased expression, including fatty acid binding protein 7 (FABP7), collapsin response mediator protein 2 (CRMP2), and cellular retinoic acid binding protein 1 (CRABP1), and seven proteins with decreased expression. In the differentiation of NS cells to neurons, we identified three proteins with increased expression, including CRMP2, and 10 proteins with decreased expression. Of these proteins, FABP7 is a marker of NS cells, CRMP2 is involved in axon guidance, and CRABP1 is thought to regulate retinoic acid access to its nuclear receptors. Western blot analysis confirmed the upregulation of FABP7 and CRABP1 in NS cells, and the upregulation of CRMP2 in NS cells and neurons. RT-PCR results showed that CRMP2 and FABP7 mRNAs were also upregulated in NS cells, while CRABP1 mRNA was unchanged. These results provide insight into the molecular basis of monkey neural differentiation.

1. Introduction

Neural stem (NS) cells have two essential characteristics, self-renewal and multipotency to differentiate into neural cells. Transplantation of neural precursors has become one of key strategies for cell replacement in the brain. A wide range of experimental approaches have been studied, but continuous expression of oncogenes or stimulation of mitogens to proliferate NS cells, in addition to the limited plasticity and slow propagation of adult stem cells, raises question about the long-term safety of the strategy [1,2]. It has been reported that the potential to maintain dying motor neurons by delivering glial cell line-derived neurotrophic factor using human adult neural progenitor cells represents a novel treatment strategy for amyotrophic lateral sclerosis [3]. In the secretome of mouse adult

Abbreviations: ES, embryonic stem; NS, neural stem; 2-DE, two-dimensional gel electrophoresis; PMF, peptide mass fingerprinting; LC-MS-MS, liquid chromatography-tandem mass spectrometry; NSS, neural stem sphere; ACM, astrocyte-conditioned medium; FGF, fibroblast growth factor; EGF, epidermal growth factor; MAP, microtubule-associated protein; GFAP, glial fibrillary acidic protein; IPG, immobilized pH gradient; IEF, isoelectric focusing; T-TBS, TBS containing 0.05% Tween; MS, mass spectrometry; ACN, acetonitrile; TFA, trifluoroacetic acid; FABP7, fatty acid binding protein 7; CRMP2, collapsin response mediator protein 2; CRABP1, cellular retinoic acid binding protein 1

* Corresponding author. Center for General Education and Department of Chemistry, Graduate School of Science, Chiba University, Yayoi-Cho 1-33, Inage-Ku, Chiba, Chiba 263-8522, Japan. Tel.: +81 043 290 2795; fax: +81 043 290 2874.
E-mail address: akama@faculty.chiba-u.jp (K. Akama).

1570-9639/$ – see front matter © 2010 Elsevier B.V. All rights reserved.
doi:10.1016/j.bbapap.2010.10.009

bone marrow stroma-derived neural progenitor cells, Prosaposin (sulphated glycoprotein 1) has been reported to protect neural cells from toxin-induced apoptotic death [4].

On the other hand, a proteomic database for NS cells isolated from the adult rat hippocampus has been developed; using a 2-DE proteomic profiling approach, about 1100 protein spots have been mapped, of which 266 have been identified [5]. In addition, a database for the expression profiling of differentiation has been developed to identify potential cellular targets mediating the differentiation of neural stem cells [6]. Furthermore, a proteome reference map of mouse NS cells and dopaminergic neurons differentiated from ES cells has been used to identify proteins with altered expression, including translationally controlled tumor protein and α-tubulin [7]. We have assessed differentially expressed genes in mouse NS cells and neurons derived from ES cells *via* the formation of neural stem spheres (NSSs), the results of which have suggested the importance of galectin 1 in regulating differentiation [8].

Less is known, however, regarding the molecular events occurring during primate neural differentiation. Differentially expressed proteins of neurons derived from human ES cells after retinoic acid induction have been identified, including α-tubulin and vimentin [9]. Moreover, 2-DE proteome analysis of a proliferating human fetal midbrain stem cell line immortalized with the v-*myc* oncogene has been used to map 402 protein spots representing 318 unique proteins, and 2-DE proteome analysis has mapped 49 protein spots representing 45 distinct proteins during differentiation into neural cells [10]. Recently, human ES cell-derived neuroectodermal spheres were found to be enriched in cytoskeleton-associated proteins [11]. Despite these findings, however, the mechanisms of differentiation from ES cells to NS cells and neurons have not been elucidated fully.

NS cells have been produced efficiently, and at high purity, from monkey ES cells (CMK6 cell line) and from mouse ES cells *via* the formation of neural stem spheres (NSSs) under free-floating conditions in astrocyte-conditioned medium (ACM), which is readily available, easy to obtain, and ready to use [12–14]. During subsequent culture of the NSSs on an adhesive substrate with FGF-2, these Nestin-positive NS cells can be induced to migrate onto the substrate, resulting in the efficient production of large numbers of NS cells. RT-PCR analysis has shown that these NS cells express NS cell marker genes such as *Pax6*, but that expression of GFAP is undetectable. Immunofluorescence analysis has shown that almost all (99.5 ± 0.5%) of the NS cells express Nestin [15]. Furthermore, almost all of these NS cells can be differentiated into functional high-molecular-mass neurofilament protein (NF-H)-positive neurons by changing the medium from Neurobasal B-27 with FGF-2 to ACM. These neurons are found to express mRNAs encoding neuron marker genes, such as *NF-H* and *MAP2*, with expression of GFAP being less than 2.6%. Immunofluorescence has shown that almost all (99.5 ± 0.5%) of these neurons expresses NF-H and tubulin-beta III, but do not express GFAP or O4 [15]. Under these culturing conditions, astrocyte-derived factors have instructed monkey ES cells to differentiate into NS cells and neurons quickly and efficiently, although we do not know what components in ACM induce the differentiation of the ES cells into neural cells [12–15], making it difficult to identify the stimulus for neurogenesis. Multitracer assessment using positron emission tomography (PET) has shown that transplantation of NS cells induced from monkey ES cells restores dopamine function in a primate model of Parkinson's disease [15].

We have used a 2-DE-based proteomic approach to identify differentially regulated proteins in monkey NS cells and neurons derived from ES cells. We found that proteins associated with signal transduction, the cytoskeleton, stress responses, and lipid metabolism were differentially expressed during the transition from ES cells to NS cells and neurons. Together with our previous report [8], these results suggest that monkey neural differentiation is regulated in a manner similar to, but somewhat different from that of, mouse neural differentiation, and that higher neural differentiation in monkeys is regulated by more proteins than in mice.

2. Materials and methods

2.1. Cell culture

The CMK6 ES cell line of cynomolgus monkey (*Macaca fascicularis*) [16] was maintained on a feeder layer of mitotically inactivated mouse embryonic fibroblasts in DMEM medium (Invitrogen) supplemented with 1 mM 2-mercaptoethanol (Invitrogen), and 15% knockout serum replacement (Invitrogen). Colonies of undifferentiated ES cells were picked up and cultured under free-floating conditions in ACM supplemented with 20 ng/ml of recombinant human fibroblast growth factor (FGF)-2 (R&D Systems, Minneapolis, MN) and 20 ng/ml of recombinant epidermal growth factor (EGF) (R&D Systems), giving rise to NSSs as described [12–15]. The NSSs were plated onto Matrigel-coated dishes and encouraged to proliferate by culturing in Neurobasal medium (Gibco Invitrogen Corp. Grand Island, NY) supplemented with 2% B-27 (Gibco Invitrogen Corp.), 20 ng/ml FGF-2, and 20 ng/ml of EGF. Following migration of the NS cells from the adhered NSS to the surrounding areas, the NSSs were removed by picking with glass capillaries, and the migrated NS cells were harvested by treatment with trypsin. The differentiation of ES cells to NS cells was dependent on ACM, and these cells did not differentiate spontaneously. Proliferation of the Nestin-positive NS cells was dependent on FGF-2 and EGF. These cells were collected by centrifugation and suspended in Neurobasal medium. To induce neuronal differentiation, the NS cells were cultured in ACM for 8 days. Proliferation of the MAP 2-positive neurons was dependent on ACM; these cells did not differentiate spontaneously.

2.2. Immunofluorescence analysis

The cells were fixed in 4% paraformaldehyde in phosphate-buffered saline (PBS). Immunocytochemistry was performed using standard protocols [12,13] and antibodies against Nestin (Rat-4-1, Developmental Studies Hybridoma Bank) and NF-H (Sigma Chemicals, St. Louis, MO). Alexa Fluor 488- and Alexa Fluor 594-labeled secondary antibodies were from Molecular Probes (Eugene, OR). Monkey NS cells and the differentiated NS cells cultured in ACM for 1–8 days were examined using a fluorescence microscope (Eclips E800, Nikon, Tokyo, Japan) equipped with phase-contrast optics.

2.3. Sample preparation for 2-D electrophoresis

Colonies of ES cells were collected by picking with glass capillaries, whereas NS cells and neurons were collected using a cell scraper. The cells were washed twice by suspending in cold PBS followed by centrifugation at 700 × *g* for 5 min, and stored as cell pellets at −80 °C. Aliquots of the cell pellets were suspended in lysis buffer containing 5 M urea, 2 M thiourea, 2% (w/v) 3-[3-cholamidopropyl]dimethylammonio]-1-propanesulfonate (Dojindo Laboratories, Kumamoto, Japan), 2% (w/v) sulfobetaine 10 (Amresco, Solon, OH), 2% Pharmalyte 3-10 (Amersham Biosciences Inc., Piscataway, NJ) without DTT, protease inhibitors (Pierce Chemicals, Rockford, IL) and phosphatase inhibitor cocktails 1 and 2 (Sigma-Aldrich, St. Louis, MO). The cell suspensions were sonicated five times on ice with 1-s bursts every 15 s at 25-W output, using an ultrasonic vibrator (UR200P; Tomy, Tokyo, Japan). The sonicated cells were centrifuged at 12,000 × *g* for 10 min, and the supernatants were ultracentrifuged at 100,000 × *g* for 30 min to remove DNA. The extracted proteins were reduced and carbamidomethylated with a ReadyPrep Reduction-alkylation kit (Bio-Rad, Richmond, CA) and desalted with a 2-D Clean-Up Kit (GE Healthcare Biosciences, Fairfield, CT) in accordance with the manufacturers' instructions. The protein content of each supernatant was measured with a 2-D Quant Kit (GE Healthcare Biosciences).

2.4. High-resolution 2-D gel electrophoresis

Proteins in the cell extract were separated according to TMIG Standard Methods in Proteomics (http://proteome.tmig.or.jp/2D/2DE_method.html) [17]. Briefly, immobilized pH gradient-isoelectric focusing (IPG-IEF) in the first dimension was performed on a reswollen Immobiline DryStrip, pH 4–7, 18 cm in length (Bio-Rad), in a CoolPhoreStar Model 3610 Horizontal IEF apparatus (Anatech, Tokyo, Japan). Aliquots of 40 μg of protein lysate per gel were loaded near the cathode wick on the IPG gel. After electrofocusing at 46,700 Vh, the IPG gel was equilibrated with SDS treatment solution (6 M urea/32 mM DTT/2% SDS/0.0025% w/v bromophenol blue (BPB)/25% v/v glycerol/25 mM Tris–HCl, pH 6.8) for 30 min. Each equilibrated gel strip was placed on top of a gel slab (7.5% T, 3% C, 20×18 cm). [%*T* means polyacrylamide gel concentration defined as percentage total monomers (i.e., acrylamide plus bisacrylamide, g/100 ml). %*C* means percentage bisacrylamide cross linker.] SDS-PAGE was run vertically in a Tris–Tricine buffer system using the CoolPhoreStar model 3068 electrophoresis apparatus (Anatech). The markers for molecular mass and p*I* were obtained from Bio-Rad and Daiichi-Kagaku (Tokyo, Japan), respectively. Proteins on gels were fixed with 40% methanol/10% acetic acid and subsequently visualized by staining with SYPRO Ruby (Molecular Probes, Eugene, OR).

2.5. Evaluation of protein patterns

2-DE gel images were scanned at an excitation wavelength of 488 nm, and emission wavelengths over 550 nm were collected on a Molecular Imager FX (Bio-Rad). Noise reduction, background subtraction, normalization, and quantitative profiling of proteins in 2-DE gels were carried out using PDQuest software version 8.0 (Bio-Rad). For spot quantification, spot volumes were calculated with the built-in feature involving the application of a fixed multiple of Gaussian radius of the spot as a background intensity function. Subsequently, relative spot intensities, defined as percentage of spot volume to the sum of total spot volumes on the parent gel, were obtained from a spreadsheet generated by the software and used for statistical analysis. All of the spots were roughly matched by an automatic program in PDQuest software, followed by a more detailed manual matching process to correct for inappropriate matching pairs, which were derived from the difference in condition of spot detection and/or the distortion of gels. Triplicate experiments were performed using three separate samples. Student's *t*-test was used to determine the significance of stage-to-stage differences. As Student's *t*-test provides valid results only when the variances of each sample are equal, a preliminary Fisher equality of variance test was applied. When variances were not equal between the two sets of data, a version of the Student's *t*-test comparison of two means including the Welch correction was used. Novel spots that appeared at a later stage were included in the comparison as increasing spots.

2.6. Mass spectrometry

In-gel digestion was performed according to the TMIG Standard Methods in Proteomics (http://proteome.tmig.or.jp/2D/2DE_method.html) [17]. Briefly, each SYPRO Ruby-stained protein spot was cut out of the gel with a spot cutter (Bio-Rad) and washed twice with 50% methanol/50 mM ammonium bicarbonate, three times with 50% acetonitrile/50 mM ammonium bicarbonate, and once with 100% acetonitrile. The supernatants were removed, and the gel fragments were dried at room temperature for 20 min. Each gel fragment was incubated in a solution of 5 μg/ml trypsin (V511A; Promega, Madison, WI) in 30% acetonitrile/50 mM ammonium bicarbonate at 30 °C overnight. The supernatants were subjected to mass spectrometry (MS). Samples (1 μl) were mixed with 1 μl of matrix solution containing 10 mg/ml CHCA (Sigma-Aldrich) in 50% acetonitrile (ACN)/40% methanol/0.1% trifluoroacetic acid (TFA), and 2-μl samples were applied to the target plate. MS analysis was performed on a MALDI-TOF mass spectrometer (AXIMA-CFR; Shimadzu, Kyoto, Japan) in reflectron mode and at a measurement range of 500–3500 *m/z*. Background noise was removed by subtraction of mass signals obtained from a control gel. Protein spots were identified by matching all the peptide masses against the Swiss-Prot and NCBInr mammal databases using Mascot Search (http://www.matrixscience.com/search form select.html) and MS Fit (http://prospector.ucsf.edu/ucsfhtml4.0/msfit.htm). In general, a mass tolerance of ±0.2 Da, one missed trypsin cleavage, oxidation of Met, and fixed modification of carbamidomethyl cysteine were selected as matching parameters in the search program.

For LC-MS-MS analysis, tryptic peptides were extracted with 0.1% TFA/2% ACN, with 0.1% TFA/33% ACN, and 0.1% TFA/70% ACN each once, respectively. The peptide extracts were dried on a speed-vacuum at room temperature. The peptides were dissolved in 2% ACN/0.1% formic acid, applied continuously to DiNa direct nano HPLC system (KYA Technologies, Tokyo, Japan) using autosampler DiNa AI (KYA Technologies), and separated with a gradient of buffer A (2% ACN containing 0.1% formic acid) and buffer B (80% ACN containing 0.1% formic acid), using a two-step linear gradient elution: 0–10 min, 100% of buffer A; 10–55 min, a linear gradient to 45% of B; 55–60 min, a linear gradient to 100% of B. The eluted peptides were injected directly into Q-TOF MS (Q-TOF Synapt; MA, Waters) through a nano-LC probe (ESI). Before each analysis, the instrument was calibrated with Glu 1-fibrinopeptide B. Erythromycin and Glu 1-fibrinopeptide B were used as references for molecular mass correction during each analysis. The collision gas used was argon. ProteinLynx Global Server version 2.3 (Waters) was used to create and search files with MASCOT search engine (version 2.2.04; Matrix Science) for peptide and protein identification. The search conditions were defined as tryptic peptides, and one missing cleavage was allowed. Carbamidomethylation at cysteine residues was selected as fixed modifications, and oxidation at methionine residues was selected as variable modifications. Precursor error tolerance and MS/MS fragment error tolerance were set to 30 ppm and 0.15 Da, respectively. Samples having total ion scores of less than 45 were rejected. The protein's name and accession number were reported based on SwissProt 56.0.

2.7. Western blotting

Following SYPRO Ruby staining, each 2-DE gel was washed three times with Milli-Q water for 30 min each. Each gel was incubated in 25 mM Tris/93 mM glycine/0.2% SDS for 15 min to resolubilize proteins, and the proteins were transferred onto PVDF membranes (Millipore, Bedford, MA) using a semi-dry electroblotting apparatus at ca. 2 mA/cm^2 for 1 h at room temperature in a buffer containing 25 mM Tris, 192 mM glycine, 0.08% SDS, and 20% methanol. The blotted membranes were rinsed twice with 10 mM Tris–HCl/150 mM NaCl/1 mM $CaCl_2$/1 mM $MgCl_2$, pH 7.4 (TBS), and blocked with 3% ECL blocking agent (GE Healthcare Biosciences)/T-TBS for 1 h. The membranes were rinsed twice with 0.05% Tween-20/TBS (T-TBS) and incubated with primary antibody overnight at 4 °C. The following primary antibodies were used: anti-FABP7 (rabbit anti-FABP7 polyclonal antibody, ab9558, 1:5000; Millipore), anti-prohibitin (goat anti-prohibitin polyclonal antibody, sc-18196, 1:5000, Santa Cruz Biotechnology, Santa Cruz, CA), anti-tubulin-β III (anti-neuron-specific class III β-tubulin mouse monoclonal antibody, TuJ-1, 1:10,000; TECHNE Corp.), anti-CRMP2 (rabbit anti-dihydropyrimidinase-related protein 2 polyclonal antibody, ab62661, 1:50,000, Abcam), anti-pCRMP2-T514 (rabbit anti-CRMP2 phosphorylated on Thr^{514} polyclonal antibody, ab85934, 1:1000, Abcam), anti-pCRMP2-S522 (rabbit anti-CRMP2 phosphorylated on Ser^{522} polyclonal antibody, CP2191, 1:500, ECM Biosciences), and anti-CRABP1 (rabbit anti-cellular retinoic acid binding protein 1 polyclonal antibody, ab62661, 1:5000, Abcam).

After washing three times with T-TBS, the membranes were incubated with appropriate horseradish peroxidase-conjugated secondary antibodies (goat anti-rabbit IgG, A 6154, diluted 1:5000 with 3% ECL blocking agent/T-TBS, Sigma; bovine anti-goat IgG, sc-2350, 1:5000, Santa Cruz Biotechnology; or goat anti-mouse IgG, A 4416, 1:5000, Sigma), followed by assay using an ECL Western blotting Detection System (GE Healthcare Biosciences).

2.8. Real-time RT-PCR analysis

Poly(A)$^+$ mRNA from undifferentiated ES colonies, NS cells, and neurons was prepared using QuickPrep Micro mRNA Purification Kits (GE Healthcare Biosciences). Each mRNA was reverse transcribed into cDNA using random hexamer primers, in accordance with the manufacturer's instructions (Applied Biosystems, Foster City, CA). Quantitative real-time RT-PCR was performed on an ABI PRISM 7300 (Applied Biosystems) using SYBR Green PCR Master Mix and the primer pairs shown in Supplementary Table 1, which had been designed using Primer Express software (Applied Biosystems), in accordance with the manufacturer's instructions. Expression of each target gene was normalized relative to that of GAPDH mRNA, with relative quantitative evaluation of the initial template copy number determined relative to a standard curve of GAPDH cDNA (Applied Biosystems). All samples were analyzed in five replicates.

3. Results

3.1. Differential expression of proteins during neural differentiation

To identify proteins that may be differentially regulated in monkey ES cells, NS cells, and neurons, we used highly homogeneous monkey NS cells expressing Nestin (99.5% ± 0.5%) and neurons expressing NF-H (99.5% ± 0.5%) differentiated from ES cells (CMK6 clone) by the NSS method [15]. Fig. 1 indicates the phase-contrast micrograph of monkey NS cells (Fig. 1A), the differentiating NS cells cultured in ACM for 1–8 days (Fig. 1B–F), and immunofluorescence analysis of the NS cells and neurons (Fig. 1G–J). The cells cultured in ACM for 8 days were differentiated to neurons. The NS cells and neurons used were confirmed to be highly homogeneous cells expressing Nestin (Fig. 1G and H) and NF-H (Fig. 1I and J), respectively, as well as the earlier report [15]. RT-PCR showed that these monkey ES cells expressed undifferentiated ES cell marker genes, such as *Oct4*, *Nanog*, and *Cripto*. Immunostaining indicated that these ES cells expressed Oct4, SSEA-1, Nanog, and alkaline phosphatase (data not shown). The monkey ES cells did not differentiate spontaneously on a feeder layer, and the levels of expression of Pax6, MAP2, and GFAP in ES cells by RT-PCR were 0.0%, 0.3%, and 0 %, respectively. RT-PCR showed that the relative levels of expression of Pax6, MAP2 and GFAP in NS cells were 100%, 4.6%, and 0 %, respectively. The relative levels of expression of MAP2, GFAP, and O4 in neurons were 100%, 2.6%, and 0 %, respectively.

Preliminary experiments using a broader pH range of pH 3–10 showed that about 2/3 of all spots of extracted proteins focused at pH 4–7 and about 1/3 at pH 7–10. However, the resolution of proteins on the gel was not fully satisfactory. We therefore used an IPG strip gel of pH 4–7 as the first step, which had a higher resolution at pH 4–7 than the strip gel of pH 3–10. Approximately 500 protein spots were detected by SYPRO Ruby staining. Using PDQuest software, quantitative comparisons were performed to assess the relative abundance of altered proteins on 2-D gel maps of the cells.

We obtained reproducible 2-DE profiles and relative spot intensities from all samples in experiments performed in triplicate. Fig. 2 shows typical gel maps of proteins from monkey ES cells, NS cells, and neurons. To assess changes in protein patterns among these three stages, we compared the patterns of ES cells and NS cells and the patterns of NS cells and neurons. Table 1 shows the relative intensities of the corresponding spots in two stages. In comparing NS cells and ES cells, we found 17 protein spots that were upregulated and seven that were downregulated. In comparing neurons with NS cells, we found three protein spots that were upregulated and 10 that were downregulated. These proteins were selected for subsequent analysis by MS. PMF and LC-MS-MS of the selected spots followed by a database search revealed the identities of these proteins (Table 1 and Fig. 2). Among the proteins upregulated when going from ES cells to NS cells were creatin kinase B type, peroxiredoxin-2, Rho GDP dissociation inhibitor 1, heterogeneous nuclear ribonucleoprotein K, vimentin, lamin B1, lamin B2, 14-3-3 protein zeta/delta, FABP7, annexin A5, reticulocalbin 1, CRMP2, and CRABP1; in contrast, heat shock cognate 71 kDa, glutathione S-transferase P, and prohibitin showed decreased expression when differentiating from ES cells to NS cells. Furthermore, in the differentiation of NS cells to neurons, reticulocalbin 1 and CRMP2 were upregulated, whereas Rho GDP dissociation inhibitor 1, annexin A5, elongation factor 1B, and heat shock protein 90B were downregulated. Table 2 summarizes the possible functions of the differentially regulated proteins during the differentiation from ES cells to neural cells. We classified the molecular functions of these proteins into eight groups: four were involved in the cytoskeleton; four, in stress responses; five, in signal transduction; and two, in lipid metabolism; the remainder were involved in protein metabolism, RNA metabolism, cell cycle, and energy metabolism.

Of the cytoskeletal proteins, lamin B1 and B2 and vimentin were upregulated in NS cells relative to ES cells. Lamin B1 and B2 are components of a fibrous layer on the inner nuclear membrane, whereas vimentin is part of the cytoskeleton, along with microtubules and actin microfilaments. Cytoskeletal networks have been reported to serve multiple roles in neurons [18]. Of the signal transduction-related proteins, Rho GDP dissociation inhibitor 1 and 14-3-3 zeta/delta were upregulated in NS cells compared with ES cells. Rho GDP dissociation inhibitor 1 has been reported to be involved in the regulation of the actin cytoskeleton [19]. It has been reported that the protein 14-3-3 zeta/delta is an adaptor protein implicated in the regulation of signaling pathways; this protein binds to and activates phosphorylated tyrosine hydroxylase, which catalyzes the rate-limiting step of dopamine synthesis [20]. Among the other proteins upregulated in NS cells and neurons compared with ES cells was reticulocalbin 1, which is thought to be involved in calcium signal modulation based on its amino acid sequence containing four EF hands (http://www.geneontology.org/).

We observed four spots of CRMP2 (Fig. 2, Table 1). Based on their electrophoretic mobility on 2-D gels [21], spots 1, 2, 3, and 4 of CRMP2 were thought to be non phosphorylated CRMP2 (CRMP2-1), CRMP2 phosphorylated at Ser^{522} (CRMP2-2), CRMP2 phosphorylated at Ser^{522} and Thr^{514} (CRMP2-3), and CRMP2 phosphorylated at Ser^{522}, Thr^{514}, and Thr^{509}/Ser^{518} (CRMP2-4), respectively. CRMP2-1 was upregulated during the differentiation of ES cells to NS cells, whereas CRMP2-2 and CRMP2-4 were upregulated from ES cells to NS cells and from NS cells to neurons. CRMP2 has been reported to be involved in axon guidance, neuronal growth cone collapse, and cell migration [22]. These findings suggest a probable link between active signal transduction and changes in the cytoskeleton during the differentiation from ES cells to NS cells and neurons. Phosphoproteomic analyses of human ES cells and during the early differentiation have suggested remodeling of the cellular matrix via active signal transduction based on changes in the proteins including cytoskeleton [23,24].

Of the heat shock/stress proteins, heat shock cognate 71-kDa protein and heat shock protein 90 beta were downregulated in neurons. Heat shock protein 90 beta, also known as tumor-specific transplantation antigen Hsp84, has been reported to inhibit tumor growth in animals injected with tumor antigen prior to tumor challenge [25]. Among the proteins involved in the redox regulation of cells, peroxiredoxin 2 was upregulated, while glutathione S-transferase was downregulated, in NS cells. Peroxiredoxin 2 has been also reported to protect neurons against peroxide [26]. Glutathione S-transferase has been reported to remove

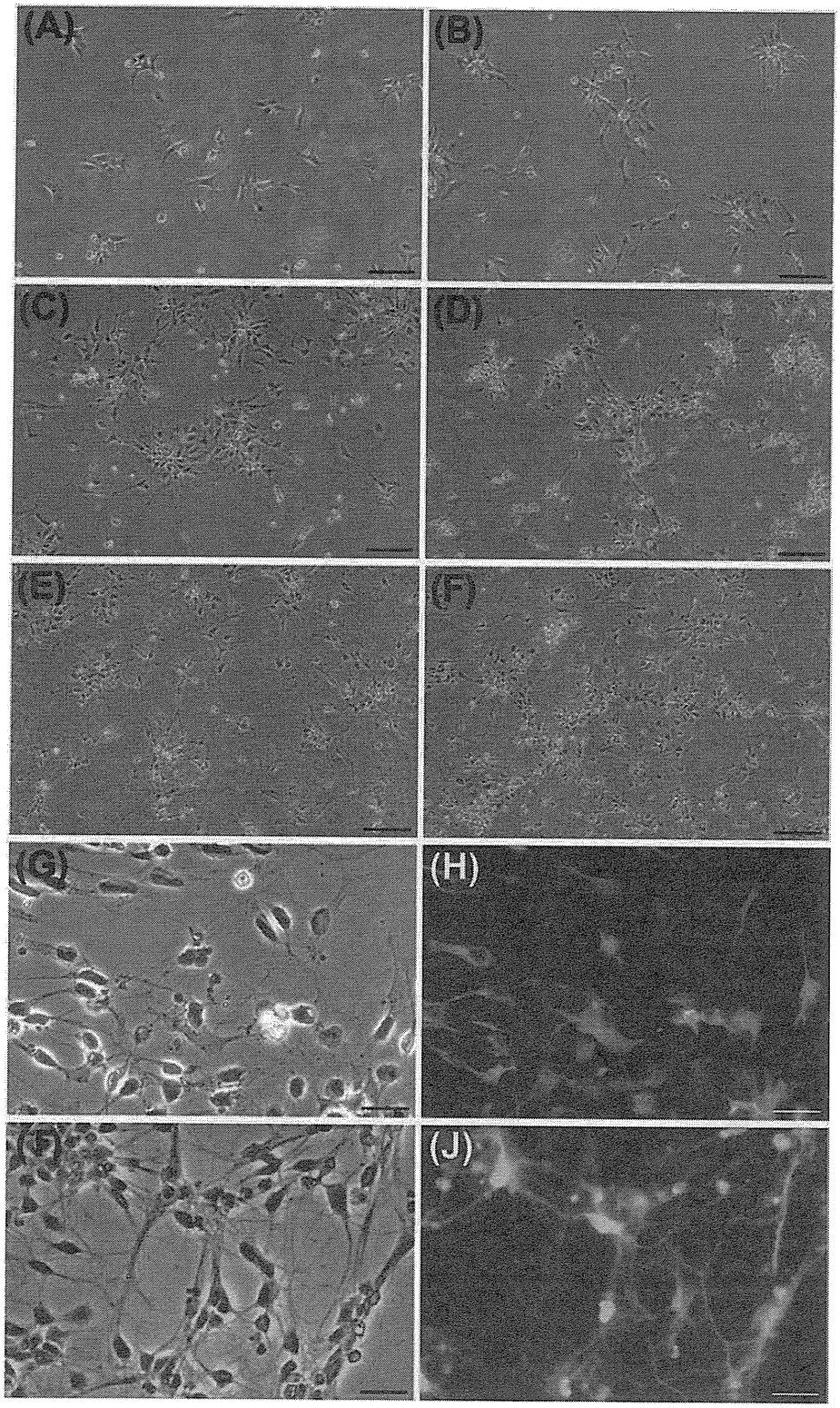

Fig. 1. Differentiation of monkey NS cells to neurons. Phase-contrast micrographs showing monkey NS cells (A), the differentiated monkey NS cells cultured in ACM for 1 day (B), 2 days (C), 4 days (D), 6 days (E), and 8 days (F). (G and I) High-magnification images of panels (A) and (F), respectively; (H and J) Nestin (orange) and NF-H (green) staining profiles by fluorescence microscope analysis of panels (G) and (I), respectively. Scale bars: (A–F) 100 μm, (G– I) 25 μm. (For interpretation of the references to color in this figure legend, the reader is referred to the web version of this article.)

wound substances by conjugation of reduced glutathione. These findings suggest that the regulation of oxidoreduction is altered in NS cells compared with ES cells.

Of the metabolism-related proteins, heterogeneous nuclear ribonucleoprotein K, which shows increased expression in NS cells compared with ES cells, has been reported to be involved in the nuclear metabolism of hnRNAs such as mRNA splicing (http://www.geneontology.org/). In contrast, both FABP7 and CRABP1 were upregulated in NS cells compared with ES cells. It has been reported that FABP7 is involved in the maintenance of NS cells and neurons [27–31], whereas CRABP1

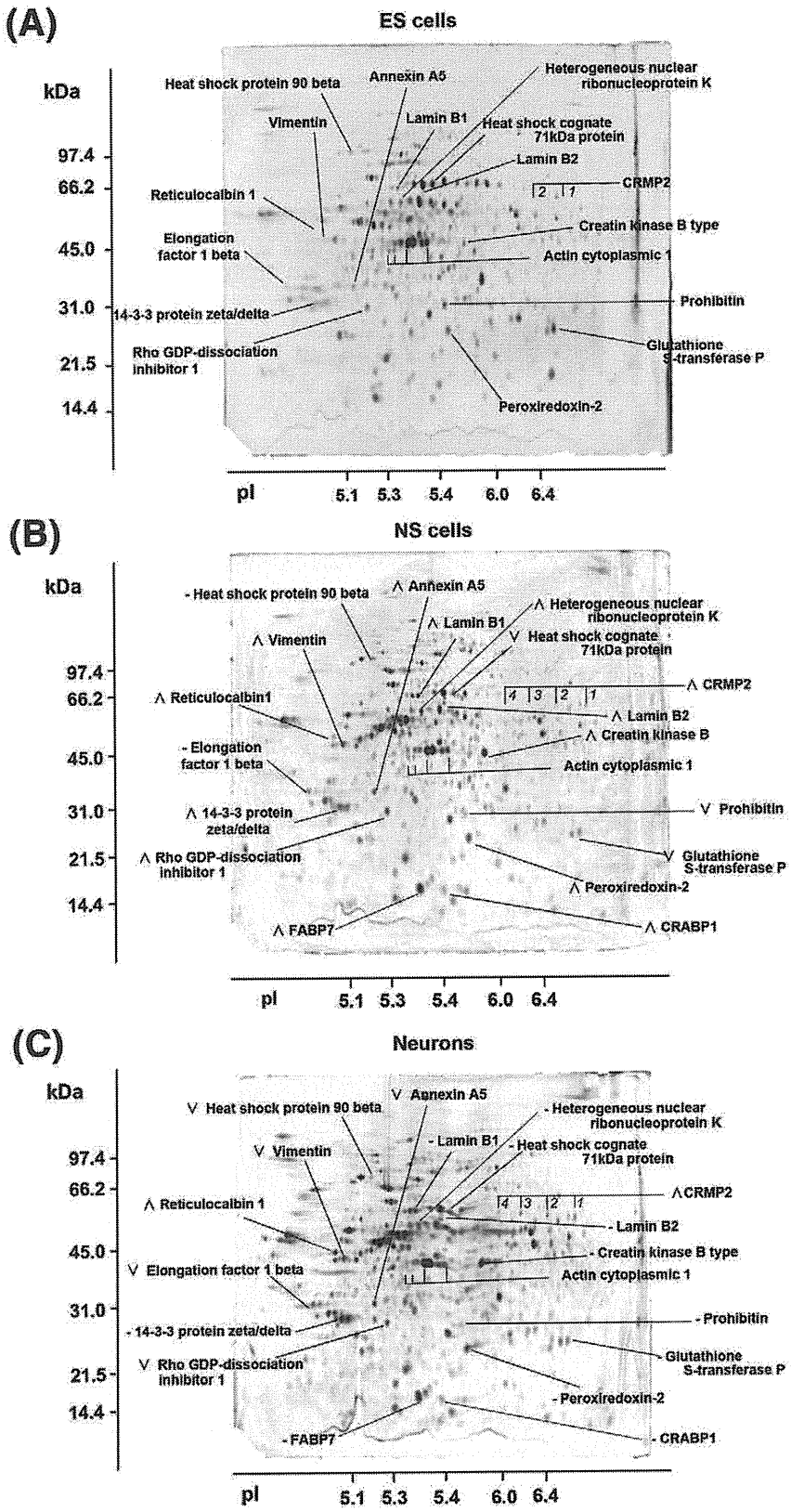

Fig. 2. 2-D protein profiles from monkey (A) ES cells, (B) NS cells, and (C) neurons. Proteins were separated based on pI (*X*-axis) and molecular mass (*Y*-axis) and visualized by staining with SYPRO Ruby. Each protein was identified by PMF and LC-MS-MS, and identified proteins with altered expression are shown on the gels. (Λ) and (V) indicate up-regulated proteins and downregulated proteins, respectively. (–) Indicates unaltered proteins.

is thought to facilitate the catabolism and/or the sequestering of retinoic acid, rendering it unavailable to nuclear receptors [32]. Retinoic acid has been reported to regulate the expression of genes involved in cell proliferation, cell differentiation, and apoptosis, and to be essential for normal embryonic development and for health in adults [33].

Table 1
Differentially expressed proteins of monkey NS cells and neurons differentiated from ES cells by the NSS method.

Ssp[a] No.	Protein name	Relative spot intensity (mean ± SD)			Quantitative changes[b]		Accession number[c]	Score[d]	Matched peptides[e]	Sequence Cov. (%)[f]
		ES cells	NS cells	Neurons	NS cells[g]	Neurons[h]				
1301	Elongation factor 1 beta	1.30 ± 0.74	1.42 ± 0.11	0.91 ± 0.19	–	−0.64 (0.05)	P24534	74/102	6/4	20/24
1309	14-3-3 Protein zeta/delta	1.78 ± 0.80	3.71 ± 0.61	4.35 ± 2.45	2.08 (0.05)	–	Q5R651	106/554	8/13	33/41
1402	Reticulocalbin 1	0.16 ± 0.14	0.98 ± 0.25	1.91 ± 0.05	6.13 (0.05)	1.95 (0.05)	Q15293	70/94	6/2	17/8
1404	Vimentin	0.31 ± 0.12	3.20 ± 0.19	2.29 ± 0.15	10.3 (0.01)	−0.72 (0.01)	Q4R4X4	213/1155	20/30	48/48
2401	Vimentin	NA[i]	3.32 ± 0.58	1.89 ± 0.24	▲ (0.05)	−0.57 (0.05)	Q4R4X4	304/861	30/25	64/48
2402	Vimentin	0.13 ± 0.18	0.89 ± 0.20	0.30 ± 0.10	6.85 (0.01)	−0.34 (0.01)	Q4R4X4	116/505	8/16	27/35
2403	Vimentin	NA[i]	2.77 ± 0.47	1.52 ± 0.05	▲ (0.01)	−0.55 (0.05)	Q4R4X4	354/1036	34/32	71/53
3508	Vimentin	0.79 ± 0.87	3.13 ± 0.90	3.53 ± 1.78	3.96 (0.05)	–	Q4R4X4	171/492	13/15	39/28
4503	Heterogeneous nuclear ribonucleoprotein K[j]	1.39 ± 0.19	1.95 ± 0.25	1.56 ± 0.72	1.40 (0.05)	–	Q4R4N6	883	25	34
2206	Rho GDP dissociation inhibitor 1	1.70 ± 0.01	2.52 ± 0.26	1.64 ± 0.17	1.47 (0.05)	−0.65 (0.01)	Q4R4J0	129/256	9/7	38/25
2303	Annexin A5	1.07 ± 0.07	1.76 ± 0.05	1.20 ± 0.20	1.64 (0.01)	−0.68 (0.05)	Q4R4H7	73/281	5/11	16/29
2702	Heat shock protein 90 beta	0.77 ± 0.18	0.74 ± 0.07	0.33 ± 0.18	–	−0.45 (0.05)	Q4R520	83/936	14/23	20/27
3306	Actin cytoplasmic 1	0.82 ± 0.03	0.53 ± 0.13	0.17 ± 0.02	–	−0.32 (0.05)	Q4L0Y2	79/155	8/6	28/21
3308	Actin cytoplasmic 1	0.87 ± 0.14	0.47 ± 0.11	NA[i]	−0.54 (0.05)	–	Q4L0Y2	68/474	5/11	16/37
4401	Actin cytoplasmic 1	4.03 ± 0.80	2.25 ± 0.28	1.22 ± 0.40	−0.56 (0.05)	−0.54 (0.05)	Q4L0Y2	105/414	8/15	24/40
5403	Actin cytoplasmic 1	4.23 ± 0.46	2.95 ± 0.32	2.48 ± 0.78	−0.70 (0.05)	–	Q4L0Y2	90/419	6/14	18/47
4201	FABP7	NA[i]	7.35 ± 1.39	7.15 ± 1.13	▲ (0.05)	–	Q15540	169/307	10/5	83/36
4602	Lamin B1	0.93 ± 0.05	1.76 ± 0.13	1.88 ± 0.04	1.83 (0.01)	–	P20700	107/1295	11/35	19/38
4611	Heat shock cognate 71-kDa protein	2.18 ± 0.22	1.50 ± 0.26	1.50 ± 0.32	−0.69 (0.05)	–	A2Q0Z1	84/813	7/25	13/31
5606	Heat shock cognate 71-kDa protein	3.28 ± 0.64	1.81 ± 0.36	2.34 ± 0.44	−0.55 (0.05)	–	A2Q0Z1	66/614	6/19	11/25
5201	Cellular retinoic acid binding protein 1	NA[i]	1.55 ± 0.37	1.15 ± 0.17	▲ (0.05)	–	P29762	119/360	6/10	48/47
5207	Prohibitin	2.05 ± 0.39	0.70 ± 0.20	0.56 ± 0.06	−0.34 (0.01)	–	Q3T165	238/283	16/8	58/36
5210	Peroxiredoxin-2	2.16 ± 0.50	3.60 ± 0.46	3.59 ± 1.37	1.67 (0.01)	–	Q5RC63	185/341	11/8	47/33
5603	Lamin B2	0.39 ± 0.11	0.71 ± 0.05	0.80 ± 0.24	1.82 (0.05)	–	Q03252	151/509	21/14	35/21
6306	Creatin kinase B type	1.14 ± 0.05	4.74 ± 0.47	4.36 ± 0.44	4.16 (0.01)	–	P12277	154/517	14/11	43/30
6614	CRMP2-4[k]	NA[i]	0.11 ± 0.04	0.36 ± 0.05	–	3.27 (0.01)	O08553	63/356	5/10	13/21
7603	CRMP2-3[l]	NA[i]	0.24 ± 0.08	0.55 ± 0.02	–	2.29 (0.05)	Q5R9Y6	108/188	9/7	21/16
8503	CRMP2-1[m]	0.16 ± 0.11	0.78 ± 0.25	1.23 ± 0.42	4.38 (0.05)	–	Q5R9Y6	121/287	12/8	25/18
8203	Glutathione S-transferase P	3.28 ± 0.23	1.55 ± 0.22	1.26 ± 0.15	−0.47 (0.01)	–	Q28514	66/306	4/7	27/38

[a] Special spot number on 2-DE gel (Fig. 2) obtained by using PDQuest software version 8.0 (Bio-Rad).
[b] The values show the fold increase of proteins toward the older developmental stage. The minus (−) values show their fold-decrease. Novel protein spots that appeared at a later stage were included in the comparison as increasing spots, and their upregulation is shown by (▲). (–): No change.
[c] Swiss-Prot accession numbers are given for proteins.
[d] Score that resulted from PMF/LC-MS-MS search (http://www.matrixscience.com/search_form_select.html) is calculated as described in the web site (http://www.matrixscience.com/help/scoring_help.html). Score in PMF is $-10*\mathrm{Log}(P)$, where P is the probability that the observed match is a random event. Protein scores greater than 61 are significant ($p<0.05$). In LC-MS-MS search, ion score is $-10*\mathrm{Log}(P)$, where P is the probability that the observed match is a random event. Individual ion scores >35 indicate identity or extensive homology ($p<0.05$). Protein scores are derived from ions sores as a non-probabilistic basis for ranking protein hits.
[e] Numbers of matched peptides that resulted from PMF/those that resulted from LC-MS-MS search obtained by using Mascot Search.
[f] Sequence coverage that resulted from PMF/that resulted from LC-MS-MS search.
[g] ES cells vs. NS cells. For protein spots that showed statistical significance, the P-values are shown in parentheses (t-test).
[h] NS cells vs.neurons. For protein spots that showed statistical significance, the P-values are shown in parentheses (t-test).
[i] NA: not detectable on the gel.
[j] Identified by LC-MS-MS search.
[k] Spot 4 of CRMP2 in Fig. 2.
[l] Spot 3 of CRMP2 in Fig.2.
[m] Spot 1 of CRMP2 in Fig.2.

3.2. Comparison of protein and mRNA expression levels

To investigate the levels of expression of the mRNAs encoding the identified proteins, we performed real-time RT-PCR analyses for reticulocalbin 1, FABP7, CRMP2, and CRABP1 [Supplementary Table 2]. Fig. 3 shows a comparison of protein and mRNA expression. The levels of expression of FABP7 and reticulocalbin 1 mRNA were altered in a manner similar to that of the respective protein expression levels (Fig. 3A, B). We found that the level of expression of CRMP2 mRNA (Fig. 3D) was upregulated from ES cells to NS cells in a similar manner to the level of expression of CRMP2-1 (non-phosphorylated CRMP2 protein). In contrast, the levels of CRMP2 mRNA were similar in NS cells and neurons, whereas the levels of expression of CRMP2-2 and CRMP2-4 proteins were increased during this differentiation step. We also found that the level of expression of mRNA encoding CRABP1 (Fig. 2C) was unchanged, differing from the changed level of expression of the encoded protein.

We found that the expression patterns of CRABP1 and CRMP2 mRNAs and proteins (Fig. 3C and D) differed. These proteins were of interest, in that they are involved in regulating neural differentiation. CRMP2 has been shown to be involved in axon guidance, neuronal growth cone collapse, and cell migration [22], whereas CRABP1 has been reported to be involved in tightly regulating the cellular concentrations of retinoic acids, which is particularly important in the development of the central nervous system [33]. We found that prohibitin was downregulated in monkey NS cells and neurons compared with ES cells (Fig. 2 and Table 1), whereas prohibitin is upregulated in mouse NS cells and neurons compared with mouse ES cells [8,34].

To confirm the differential expression of CRMP2, CRABP1, and prohibitin, we performed 2-D Western blotting analyses of these proteins, together with FABP7 and tubulin βIII as marker proteins of NS cells and neurons, respectively, using the same specimens we used for 2-DE. We found that the expression of FABP7 and CRABP1 was upregulated, whereas the expression of prohibitin was downregulated, in NS cells and neurons (Fig. 4). Western blotting analysis showed that CRMP2-1 was upregulated in NS cells, and CRMP2-2, CRMP2-3, and CRMP2-4 were upregulated in NS cells and neurons (Fig. 4E). These results were consistent with the data obtained by 2-DE except for the upregulation of CRMP2-3, which was not detected by SYPRO Ruby staining, perhaps due to overlap with other proteins.

The phospho-CRMP2 immunoblotting of neurons (Fig. 4F) indicated that CRMP2-1, CRMP2-2, and CRMP2-3 were non-phosphorylated, mono-phosphorylated on Ser^{522}, and di-phosphorylated on Thr^{514}